Removal of OMPs from WWTP Effluent: Fabrication and Application of Solar-driven Zinc Oxide/Bismuth Vanadate Photoanode

A thesis submitted in fulfilment of the requirements

for the degree of Master of Science

in Civil Engineering

by

Yiqian Wu

DEPARTMENT OF CIVIL ENGINEERING AND GEOSCIENCES

Delft University of Technology

Graduation Committee:

Prof. Dr. Ir. Jan Peter van der Hoek

Dr. Ir. Henri Spanjers

Ir. Agha Zeeshan Ali

October 2022

Certificate

It is certified that the work contained in this thesis entitled **"Removal of OMPs from WWTP Effluent: Fabrication and Application of Solar-driven Zinc Oxide/Bismuth Vanadate Photoanode"** by **Yiqian Wu** has been carried out under my supervision and that it has not been submitted elsewhere for a degree.

Prof. Dr. Ir. Jan Peter van der Hoek
Professor
Faculty CEG, Department Water Management
Delft University of Technology

Dr. Ir. Henri Spanjers
Associate Professor
Faculty CEG, Department Water Management
Delft University of Technology

Agha Zeeshan Ali
Early Stage Researcher
Faculty CEG, Department Water Management
Delft University of Technology

Declaration

This is to certify that the thesis titled **"Removal of OMPs from WWTP Effluent: Fabrication and Application of Solar-driven Zinc Oxide/Bismuth Vanadate Photoanode"** has been authored by me. It presents the research conducted by me under the supervision of **Prof. Dr. Ir. Jan Peter van der Hoek**, **Dr. Ir. Henri Spanjers** and **Ir. Agha Zeeshan Ali**.

To the best of my knowledge, it is an original work, both in terms of research content and narrative, and has not been submitted elsewhere, in part or in full, for a degree. Further, due credit has been attributed to the relevant state-of-the-art and collaborations with appropriate citations and acknowledgements, in line with established norms and practices.

Yiqian Wu
Student No. 5217806, Environmental Engineering
Faculty CEG, Department Water Management
Delft University of Technology

Abstract

Name of the student: **Yiqian Wu** Student No: **5217806**

Degree for which submitted: **Master CIE, Environmental Engineering**

Department: **Faculty CEG, Department Water Management**

Thesis title: **Removal of OMPs from WWTP Effluent: Fabrication and Application of Solar-driven Zinc Oxide/Bismuth Vanadate Photoanode**

Thesis supervisors: **Prof. Dr. Ir. Jan Peter van der Hoek**, **Dr. Ir. Henri Spanjers** and **Ir. Agha Zeeshan Ali**

Month and year of thesis submission: **October 2022**

The presence of organic micro-pollutants (OMPs) in water bodies has become a major hindrance to protecting water quality in recent years. One of the main sources of OMPs is wastewater treatment plant (WWTP) effluents. One of the most recent Advanced Oxidation Processes (AOPs) technology is photo-electrocatalysis (PEC), which can produce radicals to oxide OMPs in an aqueous medium driven by solar energy and an external bias potential. In this study, ultrasonic spray pyrolysis was determined as a proper method to fabricate the $ZnO/BiVO_4$ heterojunction. Then, the prepared photoanodes were characterised by X-ray Photoelectron spectroscopy (XPS), X-ray Diffraction (XRD), Scanning Electron Microscopy (SEM), UV-vis and Incident Photo-to-electron Conversion Efficiency (IPCE). The results demonstrated the $ZnO/BiVO_4$ heterojunction was successfully fabricated on the Fluorine-Tin-Oxide (FTO) glass. Moreover, the LSV and EIS analysis were carried out in this study to analyse its photo-electrochemical properties. The PEC degradation experiments were carried out in 10 μg/L of 11 OMPs spiked in MiliQ and in real WWTPs effluent under simulated solar illumination at 1 V potential bias for three hours. Nine and four of 11 OMPs had achieved more than 70 % degradation efficiency when

$ZnO/BiVO_4$ photoanode was conducted to degrade spiked MiliQ and spiked real WWTPs effluent. Except for diclofenac and sotalol, the real effluent showed inhibition to the degradation efficiencies and kinetic coefficient of the other nine OMPs. The concentrations of TOC, COD and NO_3-N increased after the PEC process. The increase was found to be related to the disintegration of the carbon stick cathode. To further enhance the PEC process, the $ZnO@GD/BiVO_4$ photoanode and adding persulfate were conducted the PEC degradation experiments separately in spiked real WWTPs effluent. Both two approaches showed an enhancement of the PEC process and improved degradation efficiencies. The results obtained in the present work reveal that the PEC process has excellent potential for the removal of OMPs from WWTPs effluent.

Key Words: Photo-electrocatalysis, Organic Micropollutants, Wastewater Treatment Plant Effluent.

Graphic Abstract

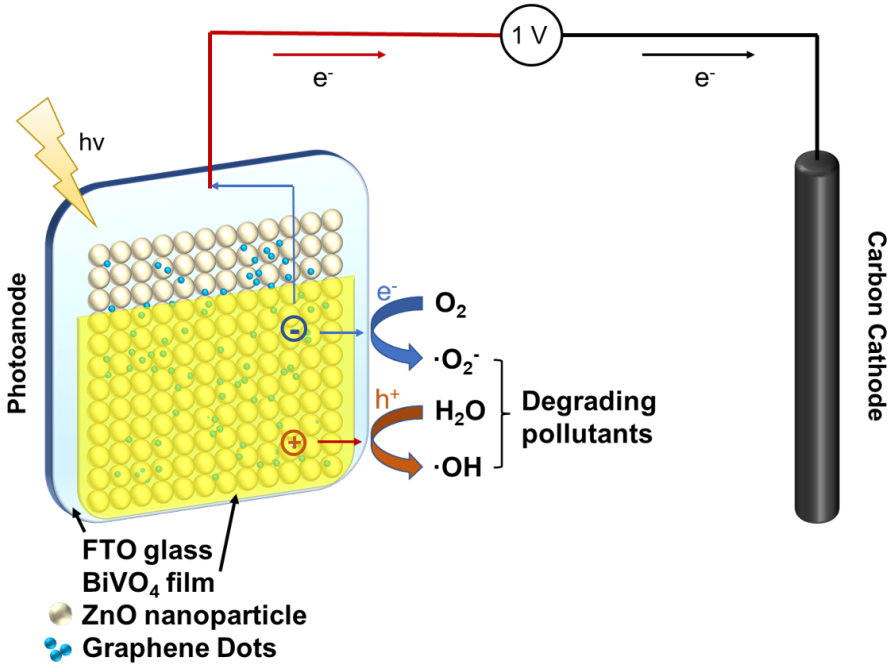

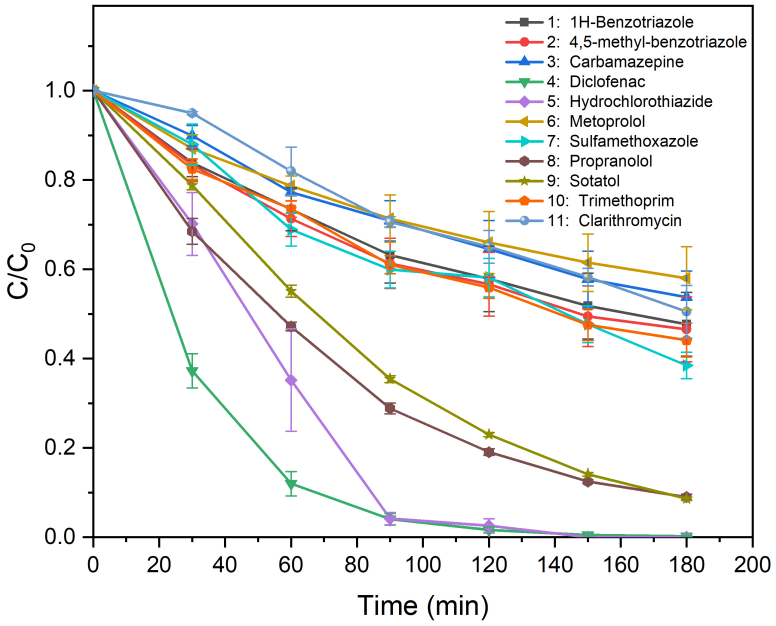

Acknowledgements

The two years I spent studying at TUD were a very valuable time in my life. I remember when I first came here, it was a very difficult time. I started living and studying in another country far away from home, and tried to take care of myself. I was under heavy pressure because of the courses and homework. But I successfully got used to life here in the second year and found myself again. The reason that I still have the courage to continue my research as a PhD student, is the support from all of the people I met in the beautiful and energetic country.

First, I am incredibly grateful to my supervisor, Prof. dr. Jan Peter van der Hoek , Dr. Ir. Henri Spanjers and Ir. Ali Agha Zeeshan. We worked together and finished two projects, my additional thesis and this thesis, which are excellent achievements for me. Every time the comments you gave me were very helpful, for both the thesis and the presentations. I was good at writing and presenting in Chinese, but everything changed when I used English. I was confused and disappointed in myself. However, All that encouragement and criticism made me improve a lot. I have been blessed to have professional and knowledgeable supervisors who are passionate about research.

In addition, I would like to especially thank my daily supervisor Ir. Ali Agha Zeeshan. We have met a lot of problems and failures in the experiment part. But after all our discussions and countless attempts, all the problems were solved. I would like to thank him for his endless patience in answering my doubts every time, even some silly ones. I was very unsure of my oral English. It was his encouragement and support that find my confidence back.

Besides, I would also like to thank my friends Yuhao Wu, Yidan Xu, Haozheng Lyu, Sandhna Jagannathan, Yejia Mao, Xinquan Lin, Connie Au, Yuhan Mao and Siyuang Wang for the accompany and the time we spent together. These times made me feel warm and happy even in a foreign country without my family. Especially, I show gratitude to Yuhao Wu, who is not only my friend but also my colleague in the same research group. We suffered the same problem here and worked together in the lab until just before locking up. He never fails to share his experimental experience with me selflessly, encouraging me every time when I was about to give up. Also, I would like to thank all current and past members of our lab for teaching experiments. Many thanks to the lab technicians for their kind help and support, who provide me with a reliable environment to do research.

Finally, I would like to show gratitude to my parents, Lin Li and Sheng Wu. They could not come to Europe because of the Covid epidemic. They still provided my tuition and expenses for living in the Netherlands and encouraged me to travel to countries in Europe. They have been of incredible love and care for me.

Everyone I have mentioned and met in the Netherlands has helped me improve, grow and become a stronger person. They made me more passionate and love about the coming life.

Yiqian Wu,
16th October, Rotterdam

Contents

List of Figures

List of Tables

Abbreviations

$OMPs$	Organic Micro-Pollutants
TPs	Transformation Products
$WWTPs$	Wastewater Treatment Plants
AOP	Advanced Oxidation Process
PEC	Photo-electrocatalysis
PC	Photocatalysis
ZnO	Zinc oxide
GD	Graphene Dots
FTO	Fluorine-doped Tin Oxide
USP	Ultrasonic Spray Pyrolysis
CNC	Computer Numerical Control
PS	Persulfate
SEM	Scanning Electron Microscopy
EDS	Energy-dispersive X-ray Spectrometer
XRD	X-ray Diffraction
XRF	X-ray Fluorescence
XPS	X-ray Photoelectron spectroscopy
$IPCE$	Incident Photo-to-electron Conversion Efficiency
LSV	Linear Sweep Voltammentry
EIS	Electrochemical Impedance Spectroscopy
DRS	Diffuse Reflectance Spectra
COD	Chemical Oxygen Demand
TOC	Total Organic Carbon

BTA	Benzotriazole
$MBTA$	Methly-benzotriazole
CBZ	Carbamazepine
DIC	Diclofenac
$HCTZ$	Hydrochlorothiazide
MP	Metoprolol
SMX	Sulfamethoxazole
PRO	Propranolol
SOT	Sotalol
TMP	Trimethoprim
CLA	Clarithromycin
$DMSO$	Dimethyl Sulfoxide
NOM	Natural Organic Matter

Symbols

$k_{\cdot OH}$	Rate Coefficient of each OMPs during the reaction with $\cdot OH$
h^+	Hole
e^-	Electron
$\cdot O_2^-$	Superoxide Radical Anion
$\cdot OH$	Hydroxyl Radical
$\cdot SO_4^-$	Sulfate Radical
R_{ct}	Charge-transfer Resistance
k	OMP degradation Kinetic constant fitted by the pseudo first order model

Dedicated to family.

Chapter 1

Literature Review

1.1 OMPs in Wastewater Treatment Plants Effluent

Nowadays, the increasing population and climte change are recognized as the most challenging problems to be faced due to the expanding demand for safe drinking water sources [3, 4]. Organic micropollutants (OMPs) originate from intense anthropogenic activities, and they have been regularly detected in wastewater treatment plants (WWTPs) effluent [5]. When OMPs enter the aquatic environment, generally through wet/dry deposition and surface runoff, they are difficult to degrade naturally because they are resistant to biotic and abiotic degradation. Thus, they can bioaccumulate in organisms higher up the food chain, threatening ecosystems, wildlife, and humans health [6].

It has been discussed that OMPs may cause hormone-disruptive effects, behavioural changes, and other potential health risks to aquatic organisms even at low concentrations (ng/L - μg/L) [7]. The potential health risk on humans of OMPs are also studied, and it has been proved that the chance of development of some diseases such as female reproductive dysfunction, adrenal and thyroid-related disorders, neuro-developmental dysfunctions in children, endocrine-related cancers and bone disorders may increase under the long-term exposure of OMPs [8]. In addition, the presence of antibiotics in waterbodies has been related to increased bacterial resistance in the environment [9].

Complete comprehension of OMP effects is missing since there is no widely agreed system to access the strength of associations between chemical exposure and adverse health effects [8]. Synergistic and antagonistic toxic effects of multiple OMP combination increase

the system's unpredictability [10]. Therefore, the existence of OMPs, including pharmaceuticals, personal care products, pesticides, and endocrine disrupting chemicals in water bodies, has drawn significant attention from the United Nations Sustainable Development Goals and the European Contaminants Watch List [11]. The existing body of research on the source of OMPs suggests that WWTPs effluent is the primary source of OMPs in water bodies compared to irrigation and runoff in agriculture activities. The WWTPs effluent is the effluent from the secondary clarifiers. However, most OMPs are difficult to remove by current primary and secondary treatment processes in conventional WWTPs due to their trace-level concentrations and a non-biodegradable and wide variety of properties [12].

The Dutch ministry of Infrastructure and Water (IenW) has listed 11 OMPs (carbamazepine, diclofenac, benzotriazole, methyl-benzotriazole, hydrochlorothiazide, sulfamethoxazole, metoprolol, sotalol, trimethoprim, propranolol and clarithromycin) as potential guide substances to monitor the effectiveness of treatment processes for OMP removal from wastewater. These target OMPs widely occur in feeding waters such as rivers, groundwater and wastewater effluents. Diclofenac and clarithromycin are on the watch list of substances for EU monitoring (Decision 2015/495/EU). As pointed out in EU Wide Monitoring Survey on Waste Water Treatment Plant Effluents [12], carbamazepine, diclofenac, benzotriazole, methyl-benzotriazole, sulfamethoxazole and trimethoprim have an extremely high frequency of occurrence in the effluents of WWTPs, with maximum concentrations over 1 μg/L.

1.2 Photo-electrocatalysis Process

To improve the degradation efficiency of OMPs, many tertiary treatment technologies such as adsorption using activated carbon [13] and membrane filtration [14] were studied. However, the treatment of the generated concentrate, as well as the aged adsorbent, will increase the complexity and cost of the overall treatment process [15]. Therefore, in this study, semiconductor photo-electrocatalysis (PEC), one of the advanced oxidation processes (AOPs), was selected to degrade OMPs due to their green and environmentally friendly properties [16].

PEC is a combination of photocatalysis and electrocatalysis processes, which has a low recombination rate of the photogenerated electron/hole pairs. The effectiveness of PEC as a powerful method for the degradation of OMPs is related to the in situ production of strong active species such as hydroxyl radicals. The mechanism of the PEC process is

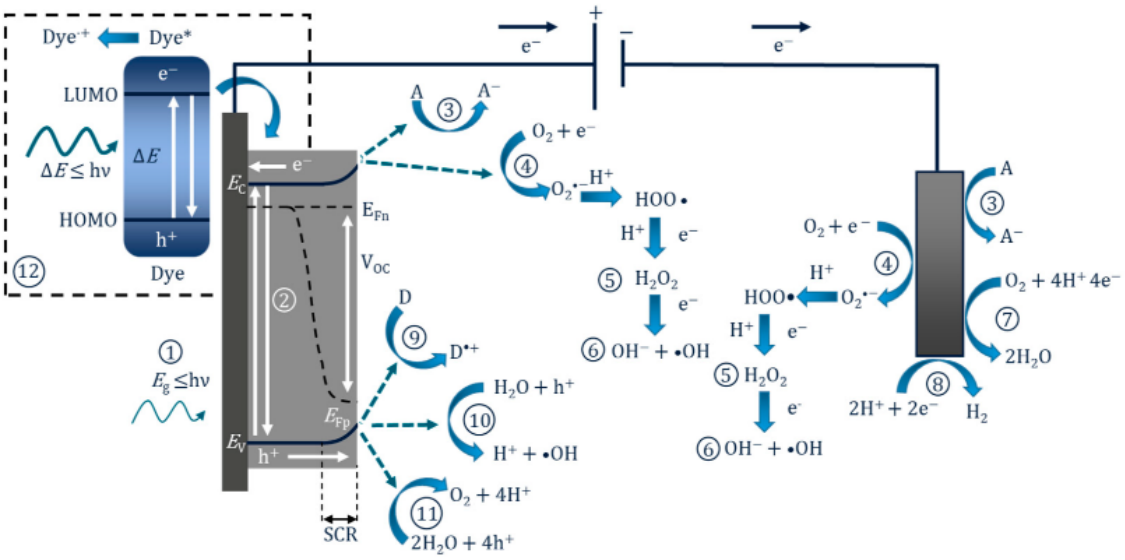

FIGURE 1.1: Diagram of the PEC process and pathways for radical production using a photoanode and a non-semiconducting counter electrode.[1]. (1) Photon absorption, (2) photoexcitation and recombination, (3) electron transfer to an electron acceptor, (4) oxygen reduction to superoxide, (5) formation of hydrogen peroxide, (6) formation of hydroxyl radical, (7) oxygen reduction to water, (8) proton reduction to hydrogen, (9) donor electron transfer, (10) oxidation of water to form hydroxyl radical, (11) oxygen evolution reaction, (12) dye sensitisation (* excited state) and electron transfer to the conduction band.

shown in Figure 1.1. Solar energy is used to irradiate the photoanode to excite electrons (which move to cathode) to the conduction band (CB) while photogenerated holes (which remain in the valence band) react with water molecules to form hydroxyl radicals [17]. Though this happens on the electrode surface, the radicals formed diffuse into the solution to react with organic molecules. Additionally, bias potential drives away electrons to the cathode and these electrons also produce superoxide radicals when they react with oxygen molecules in the solution. Therefore, the degradation of organic molecules also takes place in the bulk of the solution [17].

PEC set-up contains an external bias to semiconductor film (photocatalyst) supported on a conductive substrate (photoanode) to suppress the recombination of photogenerated electron/hole pairs. Tayebi et al. reported on applying PEC to improve the photocatalytic activity of TiO_2 [18]. The bias potential maximizes the availability of the holes generated by the photoanode, which are responsible for forming hydroxyl radicals and consequently promoting the degradation of OMPs in an aqueous medium [19]. Moreover, PEC can also generate other active species, such as superoxide radical anion, which is produced from the reaction with electrons. These oxidants increase the degradation efficiency. Tang et al. (2020) presented a PEC system to efficiently remove pollutants by different radicals,

including chloride-radical and hydroxyl radicals [20].The active species are based on the photo-electrochemical generation of highly powerful oxidizing agents able to destroy organic compounds up to their mineralization [7]. To determine the mineralization of OMPs, Nada et al. (2021) studied the PEC removal of paracetamol [21].

Only a few researchers have reported the results of PEC systems applied to real wastewater effluent treatment. These studies have used samples of municipal wastewater, and industrial water such as textile and pharmaceutical effluents [22]. A qualitative study by Cardoso (2016) described applied TiO_2 as photoanode to treat textile wastewater and compared PEC with photolysis and photocatalysis method [23]. Also, a recent study by Domínguez-Espíndola (2018) involved the PEC treatment for urban wastewater (Fecal Coliforms) by TiO_2–Ag/Al photoanode [24]. Although few studies have been reported, it is possible to affirm that PEC is an attractive method to reduce water pollution, whose study has gained strength in recent years.

1.3 Materials and Heterojunction of Photoanode

Bismuth vanadate ($BiVO_4$) is a non-toxic and low-cost semiconductor with remarkable chemical and photostability [17]. $BiVO_4$ has recently attracted wide technological applications in many fields due to its photocatalytic, acousto-optical, ferroelasticity and ionic conductivity properties [25].

Among the different crystal structures of $BiVO_4$, monoclinic scheelite has been established to possess the highest photocatalytic activity for water oxidation under visible light irradiation [26]. The energy band gap of monoclinic structure $BiVO_4$ is approximately 2.4 eV. According to the photocatalytic properties of monoclinic $BiVO_4$, it has been extensively applied in the degradation of OMPs [27, 28]. However, $BiVO_4$ suffers from excessive spontaneous recombination of photogenerated electron – hole pairs because of its narrow band gap with short hole diffusion length [29]. In addition, $BiVO_4$ has poor electron mobility and slow oxidation kinetics [30]. In order to overcome the limitations, the formation of heterojunction structure was used in this study, which is one of the effective strategies [17]. Chae et al. (2017) enhanced the light absorption of $BiVO_4$ by the WO_3 helical nanostructure and the large $WO_3/BiVO_4$ interfacial area was reported t0 contribute to efficient charge separation [31]. Guo et al. (2020) found that the photo-generated charge carriers have much longer lifetime and higher separation efficiency in $TiO_2/BiVO_4$ nanocomposite than those in TiO_2 or $BiVO_4$ alone [32].

Zinc oxide (ZnO) also has been widely studied for its application as a photocatalyst for water treatment applications. The wide use of ZnO can be rightly attributed to its properties such as ease of synthesis, non-toxicity, abundance in nature, good photocatalytic properties, large surface area, high electron mobility, remarkable thermal and chemical stability [21]. However, because of the large band gap of ZnO (3.37 eV), it performs better with UV light irradiation [33]. In order to enhance ZnO performance under visible light radiation, several strategies have been employed, such as doping with metals, metal loading, morphological control and formation of heterojunction with visible light active semiconductors [34]. For the formation of heterojunction, recent studies have found that ZnO-based heterojunctions of semiconductor (TiO2, NiO etc.)/ZnO [35], [36] could obviously suppress electron-hole pair recombination by separately transferring carriers into the heterojunction counterparts [37].

Graphene dots (GDs), as a special category of zero-dimensional (0 D) carbon nanomaterial, has ignited tremendous interest in the past few years owing to its remarkable electronic and physicochemical properties associated with edge effects [38]. GDs is featured by ultra-small particle size (< 10 nm), which affords substantially more oxygen-containing functional groups on the planar surface that can serve as highly active reaction sites [39]. Alternatively, GDs exhibit excellent solubility, chemical stability, low cytotoxicity, and high luminesce, thus providing opportunities for potential applications in a myriad of research fields [40]. In particular, the high conductivity and large specific surface area of GDs in conjunction with the various active sites on the planar surface render it a desirable and multifarious platform to integrate with diverse nanostructured materials for solar energy conversion.

The primary defect of most visible light semiconductors with a narrow band gap, such as $BiVO_4$, is the fast recombination of energetically unstable photogenerated electron-hole pairs, which inhibits their PEC progress [41]. It has been demonstrated that the construction of heterojunction is an effective way of limiting rapid recombination of charge carriers in photocatalyst by promoting effective separation of photogenerated electron-hole pairs resulting in better photocatalytic efficiency [42]. Heterojunction refers to the interface formed when two semiconductors of unequal band gap combine in such a way that it results in band alignment [43]. Heterostructure photocatalysts have been extensively applied for OMPs removal by PEC applications where higher degradation efficiencies have been recorded compared to single or pristine semiconductor [21, 44].

Chapter 2

Research approach

2.1 Research Gaps

This study will focus on solar-driven photo-electrocatalysis (PEC) technology. Based on state-of-the-art, related research was reviewed regarding OMPs in WWTPs effluent, the PEC process and the materials for photoanode. The active species produced by the photoanode have demonstrated promising results for the degradation of persistent OMPs and producing less toxic and bio-degradable products [45]. However, the following knowledge remains speculative:

1. There is a limited application of PEC in real WWTPs effluent treatment. Also, the OMP degradation is always degraded alone. Few researchers have reported the effect of degradation for OMPs in the presence of other pollutants.

2. Most of the $ZnO/BiVO_4$ heterojunction is fabricated to improve the photocatalysis process, but no literature reported coating it on a substrate to build a PEC system.

3. There is a lack of information on the effect of OMPs degradation of doped graphene dots on the PEC system.

4. Most reactors have a small volume in lab-scale experiments. Further, most studies in PEC degradation have only been carried out in high concentrations of mg/L OMPs. However, the amount of real effluent is huge and the concentration is in μg/L. These experimental results are not sufficient to provide support for practical applications.

2.2 Research Questions

Based on the knowledge gaps, the primary question of this study to be answered is:

"How to fabricate a photoanode which can be applied for the degradation of OMPs in the WWTPs effluents by solar-driven photo-electrocatalysis process? What are the degradation efficiencies of each 11 OMPs by the PEC process?"

The following sub-questions will support answering this research question:

1. What is the proper method to fabricate a photoanode with a heterojunction structure using graphene dots, ZnO and $BiVO_4$? What is the optimal fabrication sequence?
2. What is the effect of real WWTP effluent on the degradation efficiency of 11 OMPs in the PEC process?
3. What is the degradation behaviour of other pollutants in the PEC process in real WWTPs effluents?
4. How to further enhance the PEC process and improve the degradation efficiency of the 11 OMPs in real WWTP effluent?

2.3 Approaches and Hypothesis

To answer the above research questions, Table 2.1 shows the hypothesis and the approaches to test them:

2.4 Structure of the Thesis

Chapter 1 reviews in the field of photoanode fabrication and the PEC process. A brief description of the research gaps of this study, the research questions, approaches and hypothesis are given in Chapter 2. This is followed by a description of the materials of the experiment, set-up, photoanode fabrication methods, PEC degradation operations, characterization techniques and data analysis methods used in this work in Chapter 3. The results of characterization and degradation are presented and discussed in Chapter 4. Chapter 5 gives the conclusions of this research. Chapter 6. gives the recommendation based on the limitations of this study for future research. The supporting information for this study is added in the Appendices.

Table 2.1: Approaches and hypothesises related to each research question in this study.

Hypothesises	**Approaches**
Question 1 Ultrasonic spray pyrolysis can fabricate the optimal photoanode. ZnO and GDs should be fabricated first, and then $BiVO_4$ fabricated layer should be on top of it.	Conducted methylene blue degradation experiments using the photoanodes prepared by the doctor blade, electrodeposition and ultrasonic spray pyrolysis methods. Determined the optimal photoanode with the highest degradation efficiency.
Question 2 The real WWTPs effluents have an inhibition effect on the PEC process and reduce 11 OMPs degradation efficiency.	Carried out the PEC degradation experiments in spiked MiliQ and real WWTPs effluents. Compared the 11 OMPs degradation efficiencies in two solutions.
Question 3 The concentrations of TOC and COD increase, and that of NO_3-N decrease after the degradation experiments.	Measured and compared the concentration of TOC, COD and NO_3-N before and after the degradation experiment in real WWTPs effluents.
Question 4 GDs can enhance the PEC process and improve degradation efficiency. the degradation of real WWTPs effluents. Persulfate can enhance the PEC process and improve degradation efficiency.	1. GDs was doped in ZnO/$BiVO_4$ heterojunction. ZnO@GDs/$BiVO_4$ photoanode was applied in the 2. Persulfate was added to the degradation solution in the PEC process.

Chapter 3

Materials and Methods

Table 3.1 presents the 3 main parts in Chapter 3, including their methods and results.

Table 3.1: Structure of the 3 parts in Chapter 3.

Sections	**Method to select the photoanode**
Fabrication	
Doctor blade	Methylene blue degradation
Electrodeposition	Methylene blue degradation
Ultrasonic spray pyrolysis	Methylene blue degradation
Characterization	
Structural and Morphology	XRD, SEM, EDS, XPS
Photoelectrochemical properties	LSV, photocurrent, EIS
Optical properties	UV-vis, IPCE
Degradation	
In spiked MiliQ	$ZnO/BiVO_4$
In spiked real effluent	$BiVO_4$ and $ZnO/BiVO_4$
Enhanced degradation in spiked real effluent	$ZnO@GD/BiVO_4$, PS addition

3.1 Materials

The following chemical reagents were of high purity grade ($\geq 99\%$) and were used without further purification. Chemicals were used in the photoanode fabrication: p-benzoquinone was purchased from Thermo Scientific, bismuth nitrate pentahydrate ($Bi(NO_3)_3 \cdot 5H_2O$),

potassium iodide (KI), vanadyl-acetylacetonate ($VO(AcAc)_2$), sodium hydroxide (NaOH), acetic acid (CH_3COOH), nitric acid (HNO_3), sodium persulfate ($Na_2S_2O_8$), methanol, dimethyl sulfoxide (DMSO), polyethyleneglycol 200 (PEG) were obtained from Sigma-Aldrich (USA). The materials were used in photoanode preparation: zinc oxide nanoparticles (ZnO, particle diameter: ∼30 nm) were purchased from Benzeshiji Co., Ltd. (China), and graphene Dots (GDs) were purchased from Tanfeng Graphene Co., Ltd. (China, 1 mg/mL in H_2O), and fluorine-doped tin oxide (FTO) glass was purchased from Luoyang Guluo Co., Ltd. (China, 40 mm×40 mm×2.2 mm, the surface resistivity of $\sim 7\ \Omega$ /Square).

The Dutch ministry of Infrastructure and Water (IenW) has listed 11 OMPs as potential guide substances to monitor the effectiveness of treatment processes for OMP removal from wastewater. They were selected as the target OMPs in this study and their physicochemical characteristics (molecular formula, structure, CAS, molecular weight and water solubility) are shown in Fig 3.1. The target 11 OMPs in the PEC experiments: benzotriazole (BTA), methly-benzotriazole (MBTA), hydrochlorothiazide (HCTZ), clarithromycin (CLA), diclofenac (DIC), sulfamethoxazole (SMX), trimethoprim (TMP), sotalol (SOT), metoprolol (MP), carbamazepine (CBZ), propranolol (PRO) were purchased from Sigma-Aldrich (USA).

The additional chemicals used in PEC experiments: methylene blue (MB) was purchased from CZTL (UK), and sodium persulfate ($Na_2S_2O_8$) was purchased from Sigma-Aldrich (USA). The WWTPs effluent sample was taken from WWTP Horstermeer, Middenweg 159, 1394 AH Nederhorst Den Berg, Netherlands. The scheme of WWTP Horstermeer is presented in Fig 3.2. The effluent sample was taken from the discharge of the secondary settling tank. The MiliQ water used (18 MΩ/cm) was prepared by a Millipore system.

In order to minimize the error of LC-MS measurement, this study used the 0.2 μm glass fibre filter, which was purchased from ADVANTEC (Japan, GF-75, 25 mm), cooperated with the Polypropylene filter holders which were obtained from Swinnex (Germany) to filter the samples.

3.2 Fabrication

This study tested three extensively studied methods to fabricate photoanodes. The best photoanode with the highest degradation efficiency was chosen for the OMPs degradation PEC experiments in real WWTPs effluent, the experiments described in Section 3.4.2. All the FTO substrates used in this study were cleaned as follows: acetone and deionized

Chemical name	Molecular formula	Structure	CAS	pKa (at 20 °C)	Charge (at pH=7)	Molecular weight (g/mol)	Water solubility (mg/L)
Benzotriazole (BTA)	C6H4N3		95-14-7	8.37	+	119	1000-5000
Methyl-benzotriazole (MBTA)	C7H7N3		3048-48-4	8.85	+	134	1000-5000
Carbamazepine (CBZ)	C15H12N2O		298-46-4	n/a	0	236	17.7
Clarithromycin (CLA)	C38H69NO13		81103-11-9	8.90	+	797	0.33
Diclofenac (DIC)	C14H10Cl2NNaO2		15307-86-5	4.15	-	296	2.37
Hydrochlorothiazide (HCTZ)	C7H8ClN3O4S2		58-93-5	7.9	+/0	297	722
Metoprolol (MP)	C15H25NO3		51384-51-1	9.49	+	267	4777
Propranolol (PRO)	C16H21NO2		318-98-9	9.42	+	259	79.4
Sotalol (SOT)	C12H20N2O3S		959-24-0	8.3	+	308	782
Sulfamethoxazole (SMX)	C10H11N3O3S		723-46-6	5.70	-	253	500
Trimethoprim (TMP)	C14H18N4O3		738-70-5	7.3	0	290	400

FIGURE 3.1: Summary of the physicochemical characteristics of target 11 OMPs.

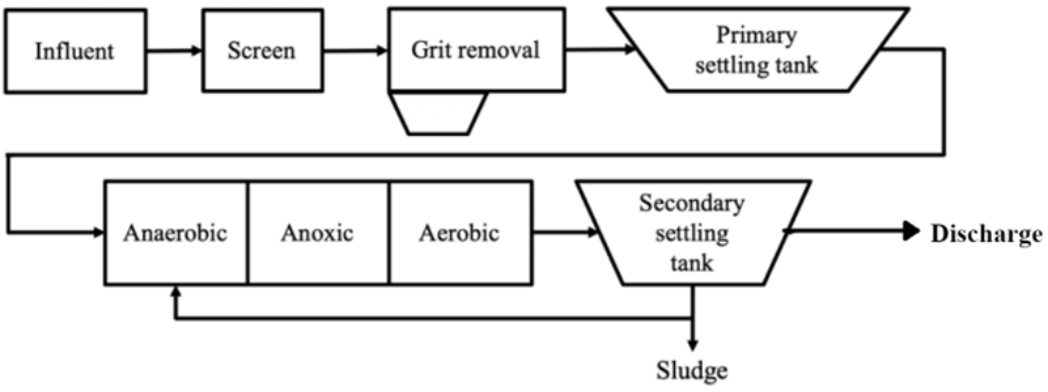

FIGURE 3.2: Scheme of WWTP Horstermeer. The effluent sample was taken from the discharge of the secondary settling tank.

water in an ultrasonic bath for 5 min each, gently raised with deionized water and dried in a fume hood.

3.2.1 Doctor Blade

The doctor blade is a convenient and efficient method for preparing the ZnO film on FTO glass [46]. Firstly, 10 mL deionized water, 10 mL ethanol, 1 mL PEG 200 and 1 g ZnO nanoparticles were mixed to prepare the ZnO paste. After that, the paste was kept under stirring overnight.

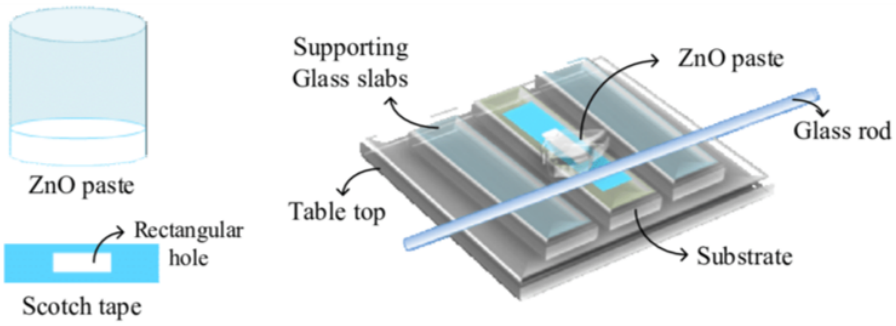

FIGURE 3.3: The ZnO thin film fabrication using doctor blade technique[2].

Secondly, the ZnO film was coated on the FTO glass. Fig 3.3 demonstrates the operation of the doctor blade technique. At first, the scotch tape was placed on the FTO glass. Then, the tabletop firmly secured the FTO glass. Two supporting glass slabs were also placed parallel with the FTO glass on the two sides. Next, 2 mL ZnO paste was dropped onto the bare substrate between the scotch tape. After that, the ZnO paste was rolled over with a glass rod to spread to the entire hole.

At last, the scotch tape was peeled off and dried the thin paste film at room temperature. Finally, the photoanode was placed in a furnace at 200 °C for 30 min (the ramping rate was 10 °C/min). When the heating process ended, it was taken out of the furnace rapidly until it cooled down to room temperature.

3.2.2 Electrodeposition

Herein, the electrodeposition method was applied in this study to obtain the $BiVO_4$ film on the prepared ZnO film. Firstly, 0.04 M $Bi(NO_3)_3 \cdot 5H_2O$ and 0.4 M KI were dissolved in the deionized water to prepare the solution A. Then, the pH was adjusted to 1.5-1.6. 0.23 M p-benzoquinone was dissolved in 20 mL ethanol to prepare solution B [47]. Solution

A and B were mixed in the ultrasonic bath to prepare the electrodeposition solution. Secondly, electrodeposition was performed potentiontatically at -0.2 V for 120 s. Fig 3.4 shows the set-up of electrodeposition, which demonstrates the positions of the working electrode, reference electrode and counter electrode in the process.

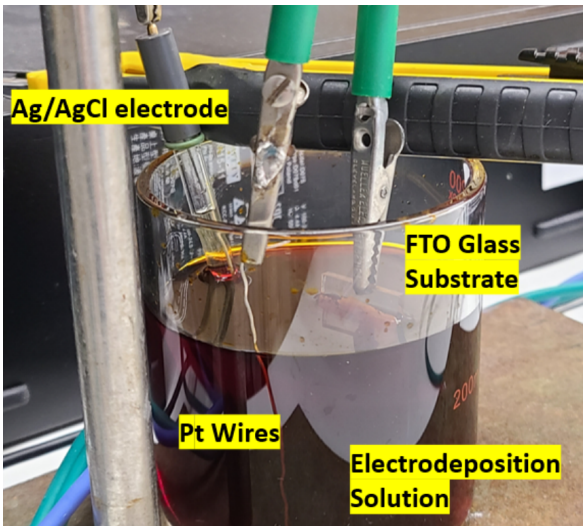

FIGURE 3.4: The three-electrodes configuration during the electrodeposition process. the FTO glass, Ag/AgCl (3.0 M KCl) electrode and platinum wire were employed as the working electrode, reference electrode and counter electrode, respectively. The prepared ZnO film faced the platinum wire.

Then, the prepared ZnO/BiOI photoanode was rinsed several times with deionized water and dried in a fume hood. A 0.4 mL of 0.20 M $VO(AcAc)_2$ (dissolved in dimethyl sulfoxide, DMSO) was drop-cast onto the surface of the ZnO/BiOI photoanode. Next, the photoanode was placed in a furnace at 460 ^oC for 2 h (the ramping rate at 2 ^oC/min). Finally, the photoanode was submerged in 1.0 M NaOH solution for 1 min with gentle stirring to remove excess V_2O_5. The resulting ZnO/$BiVO_4$ film was gently washed with deionized water and dried in the fume hood.

3.2.3 Ultrasonic Spray Pyrolysis

Compared to the doctor blade and electrodeposition, Ultrasonic Spray Pyrolysis (USP) can fabricate both thin ZnO film and $BiVO_4$ film. Also, it is convenient to fabricate most of the metal oxide film if the nanoparticles have been prepared in advance. The operation details are summarised in Table 3.2.

0.5 g ZnO nanoparticles were dispersed in 20 mL methanol to prepare the paste. The paste was kept under stirring overnight. Then, it was placed in an ultrasonic bath for 15

Table 3.2: Summary of the operation details for the UPS method.

Photoanode	**Precursor recipe**	**Heating plate temperature**	**Furnance parameters**
ZnO	0.5 g ZnO nanoparticles +20 mL methanol	60 ^{o}C	300 ^{o}C 30 min (10 ^{o}C/min)
ZnO@GD	0.5 g ZnO nanoparticles +10 mL methanol + 10 mL GDs	60 ^{o}C	300 ^{o}C 30 min (10 ^{o}C/min)
$BiVO_4$	0.02M $Bi(NO_3)_3 \cdot 5H_2O$ 10 mL acetic acid+0.02 M $VO(AcAc)_2$ 10 mL ethanol+10 mL deionized water	250 ^{o}C	460 ^{o}C 2 h (2 ^{o}C/min)

min before USP. 10 mL of the 1 mg/mL graphene dots (GDs) solutions were replaced with methanol to dop 2 % of GDs in the photoanodes.

To prepare $BiVO_4$ film by USP, firstly, 0.02 M $Bi(NO_3)_3 \cdot 5H_2O$ was dissolved in 10 mL acetic acid to prepare solution C. Then, 0.02 M $VO(AcAc)_2$ was dissolved in the mixture of 10 mL ethanol and 10 mL deionized water to prepare solution D. Solution C and D were mixed in the fume hood to prepare the solution for USP, which was homogeneous, transparent and had an aquamarine colour.

The set-up of the USP equipment is shown in Fig 3.5. Before the operations on USP, firstly, a piece of clean FTO glass was wrapped with a small strip of tin foil, about 5mm wide at its top part, to reserve a space to wire attachment. Then, the temperature of the heating plate (EQ-HP-1515-LD, MTI Corporation, USA) was settled. 60°C for ZnO film and 250°C for $BiVO_4$ film. Next, the parameters of the X-Y axis computer numerical control (CNC) machine (MSK-Uwith a small strip of tin foil SP-ST1, MTI Corporation, USA, the one at the bottom) were adjusted. In the fabrication process, the moving speed of the plate was 30 mm/min on the x-axis. A syringe pump (NE-1010, ProSense B.V., the Netherlands) with a 30 mL syringe was placed to control the output speed of the precursor, which was adjusted to 0.05 mL/min. It pumped the precursor to the ultrasonic nozzle, which was positioned 8 cm directly above the FTO substrate. The ultrasonic nozzle separated the incoming precursor into nano drops by 0.05 W ultrasonic (created by the ultrasonic generator above CNC, MSK-SP-01A, MTI Corporation, USA). The airflow blew the nano drops out of the ultrasonic nozzle to the FTO glass lying on the plate.

Finally, the prepared photoanodes were placed in the furnace. The temperature was settled on 300 ^{o}C for 30 min at 10 ^{o}C/min ramping rate to anneal ZnO and ZnO@GD film, 460 ^{o}C for 2h at 2 ^{o}C/min ramping rate to anneal $BiVO_4$ film.

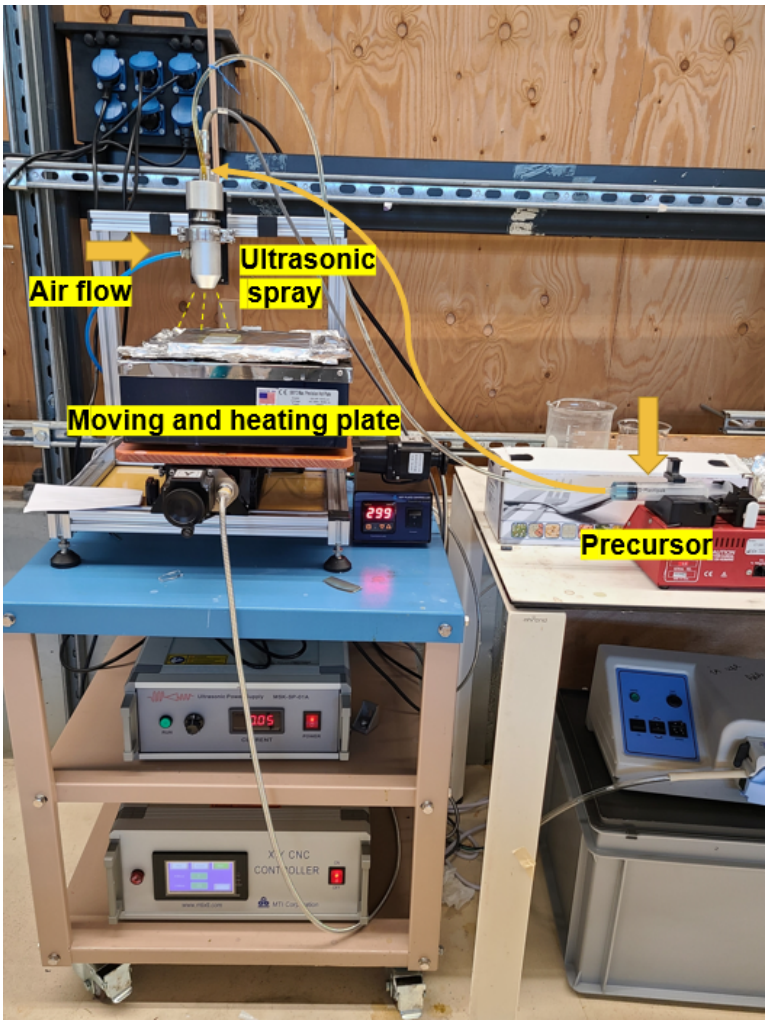

FIGURE 3.5: The set-up of the Ultrasonic Spray Pyrolysis (USP).

3.3 Characterization Methods

To characterize the structural and morphology properties of photoanodes, the following analyses were carried out: scanning electron microscopy (SEM) (FEI, Quanta F650) coupled with an energy-dispersive X-ray spectrometer (EDS, FEI Model Quanta 650 Field Emission Scanning Electron Microscope, Inca 250 SSD XMax20 detector). The degree of crystallinity and purity of the photoanodes were determined with the X-ray diffraction (XRD) using Cu Kα radiation within a range of 2 θ = 10 ^{o} - 130 ^{o}, a step size of 0.040 ^{o} 2 θ, and counting time per step 2 seconds. And the elements of the photoanodes were determined by X-ray fluorescence (XRF) (Panalytical Axios Max WD-XRF spectrometer, SuperQ5.0i/Omnian software). In order to determine the improvement when attaching GD to the photoanode, the X-ray photoelectron spectroscopy (XPS) analysis was carried

out with a Thermo Fisher K-Alpha surface analysis machine (Thermo Fisher Scientific, USA) to determine the binding energy of each element. Further, the UV-vis (LAMBDA 1050+ UV/Vis/NIR spectrophotometer, UV Winlab software) and incident photon-to-electron conversion efficiency (IPCE) was applied to determine the enhancement of solar conversion by GD [48]. The radiation wavelength range for both analyses went from 280 nm to 700 nm.

The photoelectrochemical and electrochemical properties of the photoanodes were analysed by linear sweep voltammetry (LSV) and electrochemical impedance spectroscopy (EIS). The measurements were carried out in 0.2 M Na_2SO_4 solution. For LSV analysis, the bias potential was tested from -0.2 V_{REF} to 2 V_{REF}, at a 0.1 V/s scan rate in both dark and light conditions. For EIS analysis, the applied frequency was carried out from 10000 Hz to 0.01 Hz, plots were obtained under both dark and light conditions at room temperature.

3.4 Photo-electrocatalysis Degradation Experiments

3.4.1 Photo-electrocatalysis Process Set-up

All the photocurrent and current data were recorded on an Autolab PGSTAT128N (Netherlands) machine with a two-electrodes configuration. And all photo-electrocatalysis (PEC) Process was carried out in the set-up shown in Fig 3.6. The volume of the reactor was 147 mL. A magnet stirring bar was placed at the bottom of the quartz cell at 150 rpm to create enough turbulence inside. The prepared photoanode and carbon stick electrode were performed as a working electrode and a counter electrode, respectively. The solar simulator (Atlas, SUNTEST XXL+, USA) with three air-cooled 1700 W Xenon lamps (60 W/m^2) was used in this experiment.

3.4.2 Methylene Blue Degradation

The methylene blue degradation experiment was designed as a pre-experiment for the OMPs degradation part. It was aimed to determine which method can fabricate a photoanode that both have high degradation efficiency and can be used many times. Then this photoanode would be applied in real effluent treatment in the following experiments. First, 2.5 mg/L methylene blue solution was prepared in deionized water and analyzed at 664 nm. The calibration curve was plotted in Fig 3.7.

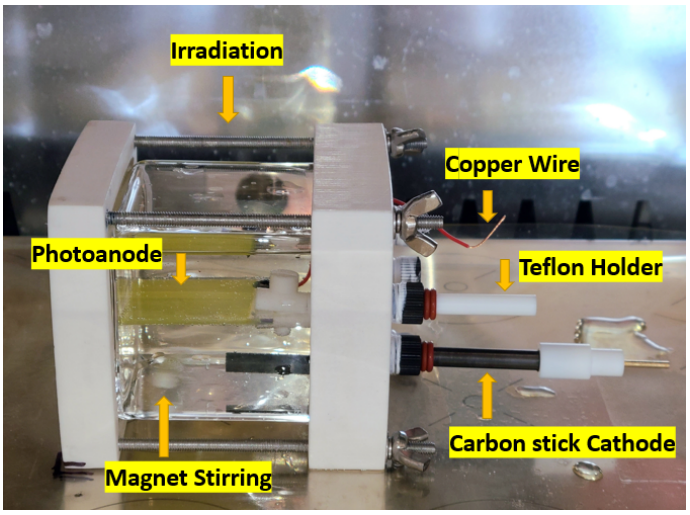

FIGURE 3.6: The set-up of a two-electrodes configuration for photo-electrocatalysis (PEC) process.

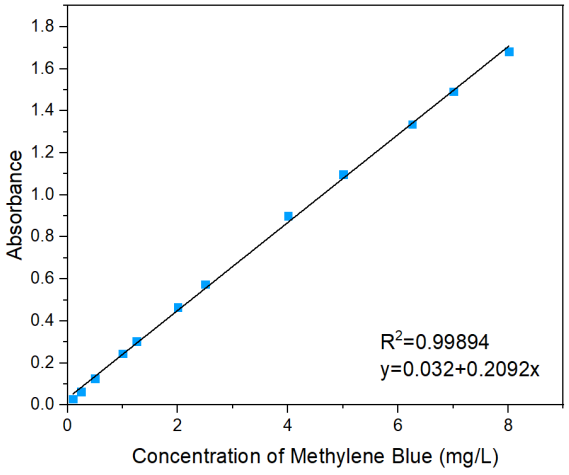

FIGURE 3.7: The calibration curve of methylene blue at 664 nm.

The prepared photoanode was applied in the degradation of 147 mL 2.5 mg/L methylene blue and 0.1 M Na_2SO_4 solution in the PEC set-up mentioned above. First, the photoanode was submerged in the solution in a dark condition at 150 rpm stirring for 15 min. The simulated solar was produced by SUNTEST XXL+ (60 W/m^2). Autolab recorded the current data at 1 V bias potential. A 1.5 mL water sample was taken at the beginning and every 15 min in one hour PEC process, measured the samples at a 664 nm spectrophotometer. The degradation efficiency was calculated using Equation 3.1.

$$Degradation\ Efficiency\ (\%) = (1 - \frac{Measured\ Concentration(C)}{Initial\ Concentration(C_o)}) \times 100$$
$$Total\ Degradation\ Efficiency\ (\%) = (1 - \frac{Measured\ Concentration(C)}{Final\ Concentration(C_{after})}) \times 100 \tag{3.1}$$

After the 3 h PEC process, the total degradation efficiencies of different photoanodes were calculated using Equation 3.1. The photoanode with the highest total degradation efficiency was chosen to conduct the PEC process in the real WWTPs effluents degradation part.

3.4.3 MilliQ degradation experiments

Before applying the chosen photoanode in real WWTPs effluent treatment, the PEC process was first carried out in the spiked ultrapure water with eleven OMPs. The MiliQ was spiked with 1 mg/L of 1H-benzotriazole (BTA), 4,5-methyl-benzotriazole (MBTA), carbamazepine (CBZ), diclofenac (DIC), hydrochlorothiazide (HCTZ), metoprolol (MP), sulfamethoxazole (SMX), propranolol (PRO), sotalol (SOT), trimethoprim (TMP) and clarithromycin (CLA). The spiked solution contained 10 μg/L of 11 OMPs. First, the photoanode was submerged in the solution in a dark condition and kept magnetic stirring for 15 min. Autolab recorded the photocurrent data at 1 V bias potential. 1 mL water sample was taken before the PEC process as the original sample. Then, 1 mL water sample was taken every 30 minutes during the three-hour PEC process in the setup mentioned in Section 3.4.1.

3.4.4 Real WWTP effluent Degradation

The WWTPs effluent sample was taken from WWTP Horstermeer, Netherlands, in both June and July 2022. The PEC degradation of real effluent was under the same operations of MiliQ experiments in Section 3.4.3. 1 mL sample was taken every 30 min in three hours PEC process.

Three methods were tested in this study to further enhance the PEC process and increase the degradation efficiency in real effluent treatment. (1) Weight ratio of 2% GDs was doped in the ZnO paste to fabricate a ZnO@GD/$BiVO_4$ photoanode. These experiments were

carried out under the same operations as above. (2) 1 mM sodium persulfate ($Na_2S_2O_8$, PS) was added into the solution to produce sulfate radicals and enhance degradation efficiency. 1 mL sample was taken before and after adding PS and at minutes 5, 10, 15, 20, 30, 45 and 60 of the one-hour PEC process.

3.5 Analytical Methods

3.5.1 OMPs analysis

The concentrations of 11 OMPs were measured by high-performance liquid chromatography combined with tandem mass spectrometry (LC-MS). To prepare the LC-MS sample, firstly, the obtained 1 mL water sample was diluted to 3 mL with MiliQ. After the diluted samples were shaken well, they were filtered with a 0.2μm glass fibre filter (ADVANTEC, GF-75, 25 mm). The first 1.8 mL filtered diluted sample was discarded. Then, the left 1.2 mL sample was injected into a valve. Finally, 495 μL filtered solution and 5 μL internal standard solution were mixed in another valve and shaken well again. Every sample was marked and stored in a fridge if needed.

3.5.2 Other pollutants analysis

Three of the most common chemical contaminants of water were measured to analyse the degradation from another perspective. The Chemical oxygen demand (COD), total organic carbon (TOC) and Nitrate-Nitrogen (NO_3-N) concentration were measured by HACH LCK 339 Nitrate (0.23-13.50 mg/L NO_3-N, USA) HACH LCK 314 COD (15-150 mg/L O_2, USA). TOC-V CPH/CPN (Shimadzu, Japan), respectively, before and after degradation. The pH and electrical conductivity (EC) were measured by pH and EC meter (Shanghai Bante M852, China).

Chapter 4

Results and Discussions

4.1 Photoanode Selection Results

The methylene blue degradation was carried out as the pre-experiments for the OMPs degradation. This study first fabricated ZnO film by the doctor blade method. Then the $BiVO_4$ film by electrodeposition method. As shown in Fig 4.1 (a), the white ZnO film was thick and opaque. After applying this thick film to the methylene blue degradation experiment, this thick film was fragile and prone to breakage due to the water flow inside the PEC reactor, which can be seen in Fig 4.1 (b). Another problem was found in this experiment, as presented by Fig 4.1 (c), that the $BiVO_4$ film cannot be evenly distributed on ZnO film by the electrodeposition method. In this case, the heterojunction of ZnO and $BiVO_4$ cannot be fabricated by the doctor blade and the electrodeposition methods, no matter which layer was on the top or the bottom.

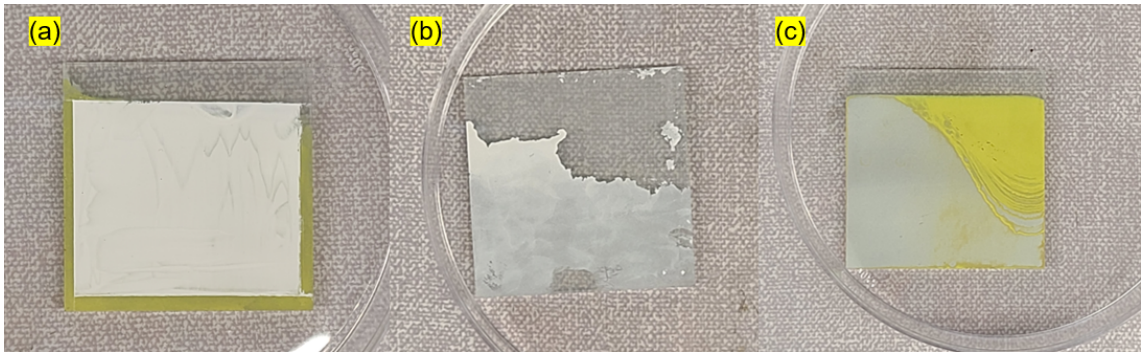

FIGURE 4.1: The photos of (a) electrodeposited $BiVO_4$ film at the bottom, ZnO film on the top by the doctor blade, (b) the broken ZnO film after the PEC degradation experiment, (c) the unevenly distributed $BiVO_4$ film on ZnO film by electrodeposition.

Next, ultrasonic spray pyrolysis was used to fabricate both ZnO and $BiVO_4$ film. In order to determine which material should be on the top and at the bottom, the pure ZnO, pure $BiVO_4$, $BiVO_4$(bottom)/ZnO(top), and ZnO(bottom)/$BiVO_4$(top) were tested in the PEC degradation experiments. These experiments were carried out in the 2.5 mg/L methylene blue and 0.1 M Na_2SO_4 solution, applied 1 V bias potential. Within the one-hour PEC process, the methylene blue degradation efficiencies were shown in Fig 4.2 (a). However, the pure ZnO had the highest degradation efficiency. One reason why ZnO film was the best could be the film is fragile and the water flow produced by magnet stirring would bring the ZnO particles as the photocatalyst full filled the reactor. As the consequence, there was a photocatalysis process instead of a PEC process. Further, the contact area of the catalyst multiplied because the film was broken into tiny pieces, which were more like slurry.

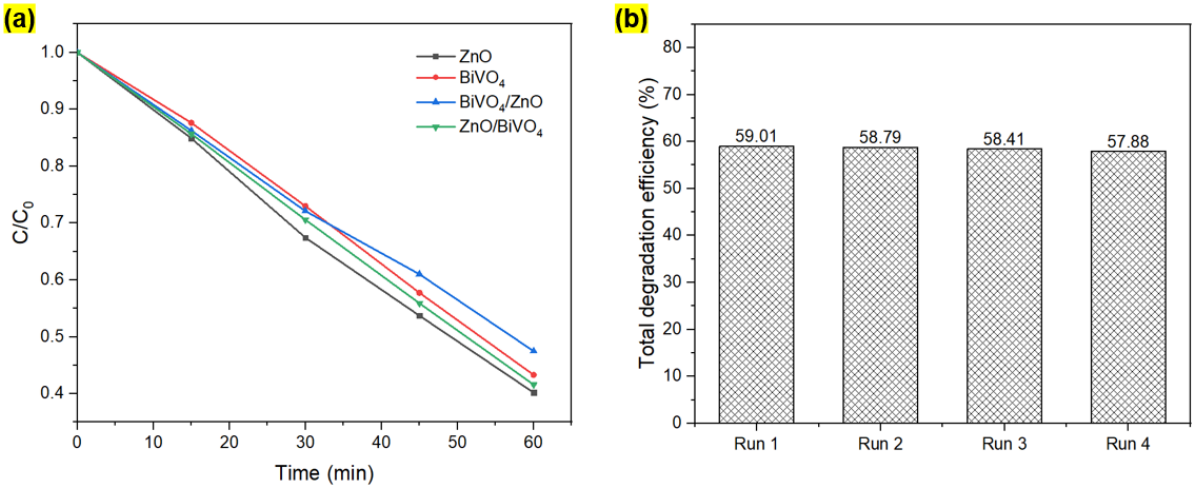

FIGURE 4.2: The plots of (a) the degradation efficiencies of the pure ZnO, pure $BiVO_4$, $BiVO_4$(bottom)/ZnO(top), and ZnO(bottom)/$BiVO_4$(top) photoanodes versus time, (b) the total degradation efficiencies in four batch runs carried out by the same ZnO(bottom)/$BiVO_4$(top) photoanode.

As the photoanode which had the second highest degradation efficiency, ZnO(bottom)/$BiVO_4$(top) was selected and repeated three more batch runs of the PEC experiments under the same conditions. As shown in Fig 4.2 (b), in the first batch run, the total removal efficiency of methylene blue was 59.01%. It decreased to 57.88% in the fourth run, which only had a 2% loss. Therefore, the ZnO(bottom)/$BiVO_4$(top) film was strong enough to repeat the PEC process. One reason could be that the $BiVO_4$ film was strong and protected the ZnO particles underneath. This phenomenon has been proved by the results of SEM in Section 4.2.2.

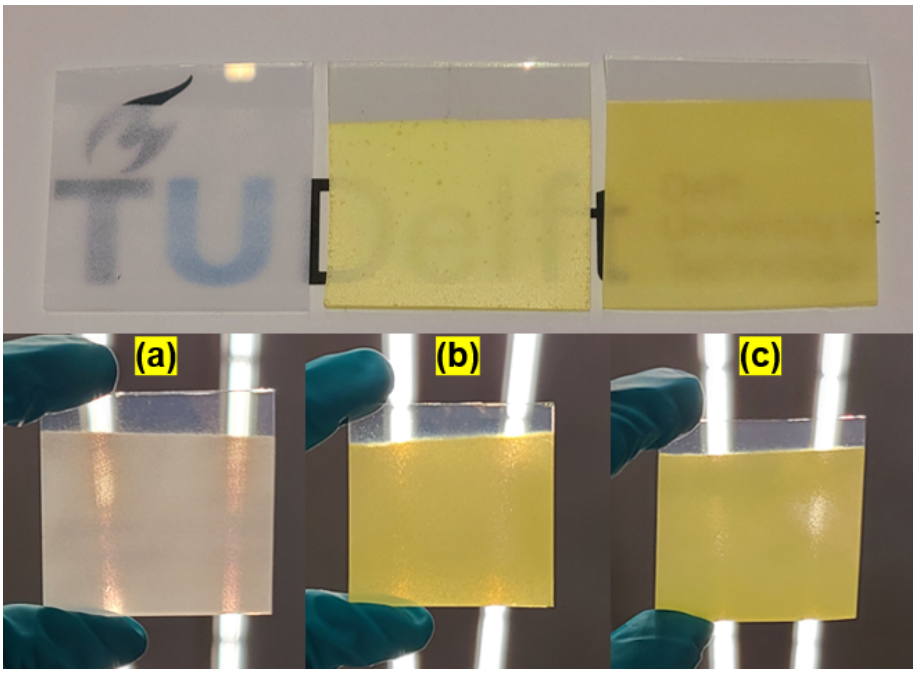

FIGURE 4.3: The pictures of (a) ZnO, (b) $BiVO_4$, (c) ZnO/$BiVO_4$ photoanodes on the paper and under the LED light.

Fig 4.3 shows the photoanodes fabricated by the USP method. Each of them was semi-transparent, homogeneous and evenly distributed, but only the $BiVO_4$ and ZnO/$BiVO_4$ photoanodes were strong enough to be applied in the subsequent degradation experiments.

4.2 Strualctural and Morphology Characterization Results

4.2.1 XRD analysis

X-ray Diffraction (XRD) pattern analysis of bare FTO, pure $BiVO_4$, pure ZnO and ZnO/$BiVO_4$ are shown in Fig 4.4. Both diffraction peaks of $BiVO_4$ and ZnO can be indexed as monoclinic scheelite of $BiVO_4$ phases and hexagonal wurtzite crystal planes of ZnO phases and matched well with a JCPDS no. 75-1866 and JCPDS no. 083-1699, respectively [49, 50]. The XRD pattern values at 18.7^o, 19.0^o, 28.9^o, 30.5^o, 34.5^o, 35.2^o, 39.7^o, 42.4^o, 46.7^o, 47.2^o and 50.2^o corresponds to (101), (011), (112), (040), (200), (002), (211), (015), (204), (024), (116) planes respectively of monoclinic scheelite $BiVO_4$ is perfectly matched the standard [50]. For the hexagonal wurtzite crystal planes of ZnO, the main peaks at 31.92^o, 34.45^o, 36.34^o, 47.63^o, 56.68^o, 62.94^o,66.11^o, 68.16^o and 69.10^o correspond to (100), (002), (101), (102), (110), (103), (200), (112) and (201) planes [49].

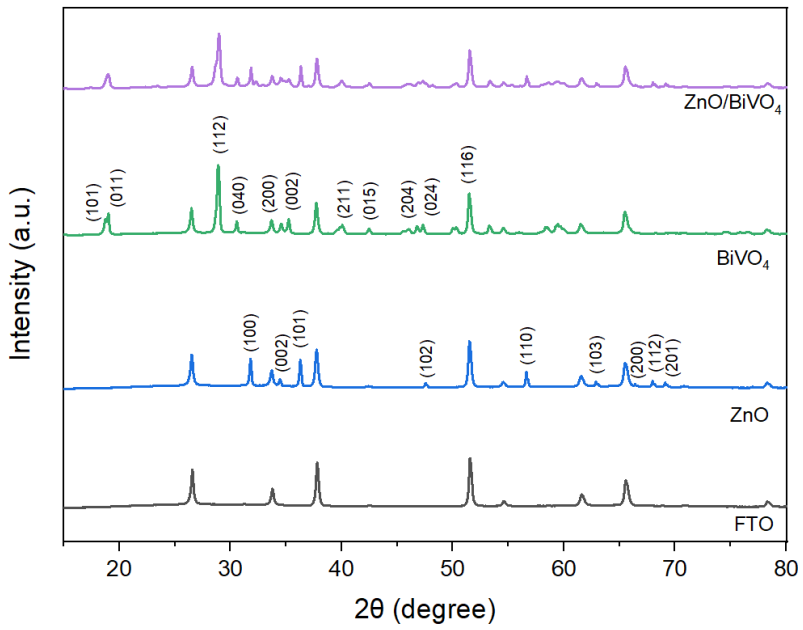

FIGURE 4.4: XRD patterns of the bare FTO, pure $BiVO_4$, pure ZnO and ZnO/$BiVO_4$ photoanodes

Further, XRD analysis presents that the characteristic peaks of bare FTO, pure $BiVO_4$ and pure ZnO photoanodes were all observed in ZnO/$BiVO_4$ photoanode. Therefore, the heterojunction of ZnO/$BiVO_4$ was successfully fabricated. Besides, no other impurity peaks were found, which means the pure phase and high crystallinity were achieved in this study.

4.2.2 SEM and EDS analysis

Scanning Electron Microscopy (SEM) images were obtained to study the morphological characterizations of bare FTO glass, pure $BiVO_4$, pure ZnO and ZnO/$BiVO_4$ photoanodes. When fabricated $BiVO_4$ film by electrodeposition method, the coral-shaped $BiVO_4$ was obtained in our previous study [51]. This study used USP to fabricate the $BiVO_4$ film, its low and high magnification SEM images are shown in Fig 4.5 (a) and (c). However, the $BiVO_4$ film is more like a coral-shaped cross-section compared to the $BiVO_4$ film fabricated by the electrodeposition. This brain-shaped pattern of USP $BiVO_4$ film was also reported by Kim et al. (2016) [52]. Therefore, the USP one was thinner and more compact, but with less contact area.

The low and high magnification SEM images of the ZnO photoanode are shown in Fig 4.5 (b) and (d). The diameter of the ZnO particles was about 30 nm. Hence, the USP ZnO

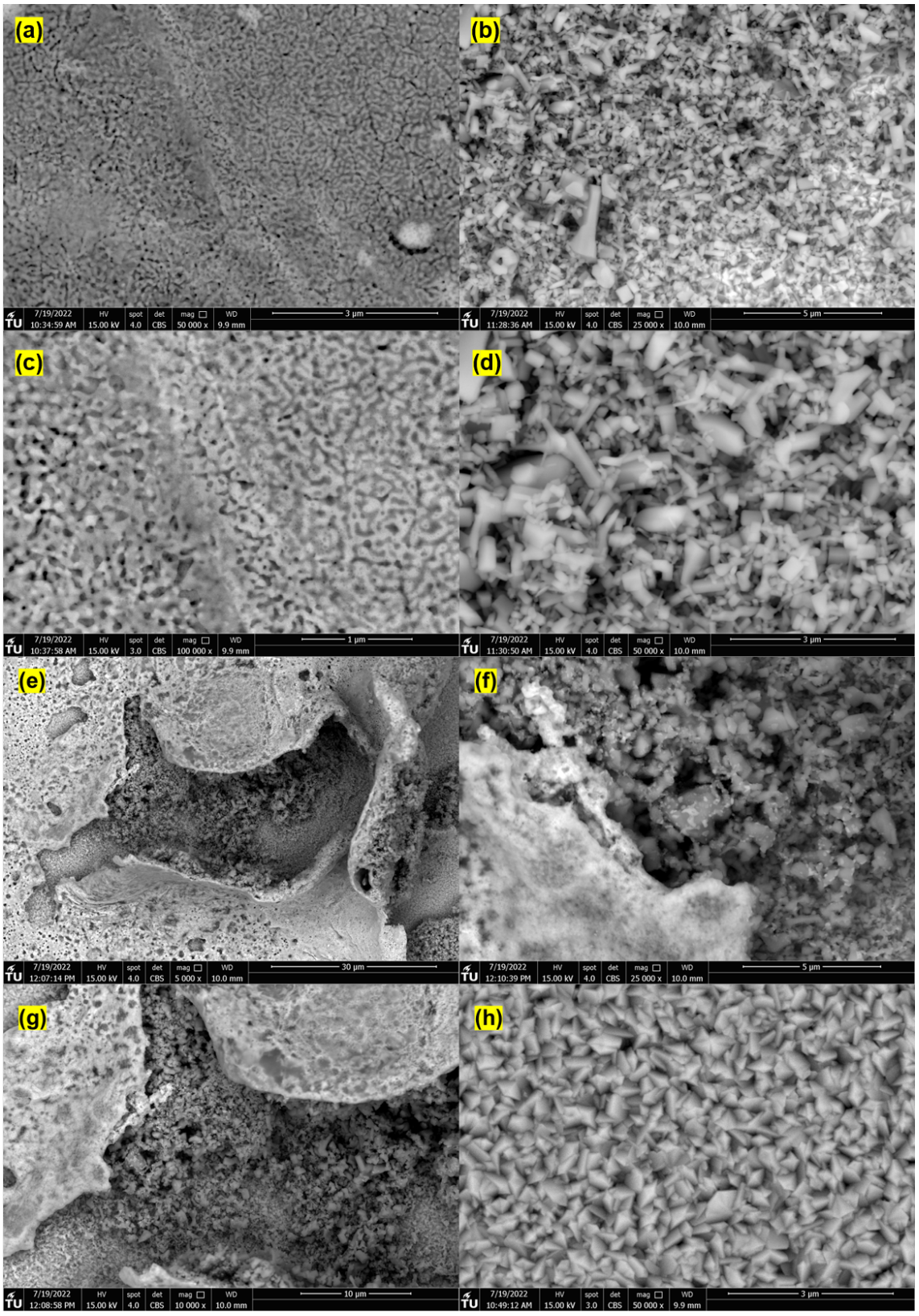

FIGURE 4.5: Low and high magnification SEM images of (a) 50 000x $BiVO_4$, (b) 25 000x ZnO, (c) 100 000x $BiVO_4$, (d) 50 000x $BiVO_4$, (e) 5000x $ZnO/BiVO_4$, (f) 25 000x $ZnO/BiVO_4$, (g) 10 000x $ZnO/BiVO_4$ photoanodes, (h) 50 000x bare FTO glass.

particles were piled on top of the FTO glass. Therefore, water flow can easily take the ZnO particles away from the FTO substrate. This problem also accords with our earlier observations in Section 4.1, which showed that the ZnO photoanode had the highest methylene blue degradation efficiency. It was because the ZnO particles left the substrate and distributed throughout the entire degradation solution under the photocatalysis process.

According to the degradation results in Section 4.1, ZnO/$BiVO_4$ film was strong enough to be reused. The SEM images of ZnO/$BiVO_4$ photoanode focus on a small crack which is shown in Fig 4.5 (e), (f) and (g). The thin $BiVO_4$ film covered the ZnO particles. Moreover, the thin $BiVO_4$ film acted as a protection layer, preventing ZnO particles from taking away by the water flow. Despite ZnO having good photostability, high carrier mobility and conductivity as a semiconductor [53], it dissolves readily in acidic and alkaline solutions. Therefore, coating $BiVO_4$ on top of it is difficult. However, acetic acid was used in the precursor of the $BiVO_4$ aimed to solve this problem. When the $BiVO_4$ precursor was sprayed on the ZnO film, part of the ZnO would react with acetic acid and transform into zinc acetate ($Zn(CH_3COO)_2$). Further, $Zn(CH_3COO)_2$ was pyrolysed and transformed back to ZnO in the furnace under 460 ^oC [54, 55]. The chemical reactions are shown in Equation 4.1.

$$\begin{aligned} 5Zn(CH_3COO)_2 \cdot H_2O &= Zn_5(OH)_8(CH_3COO)_2 + 2CH_3COOH \\ Zn_5(OH)_8(CH_3COO)_2 &= 5ZnO(s) + 2H(C_2H_3O_2^-)(g) + 3H_2O(g) \end{aligned} \tag{4.1}$$

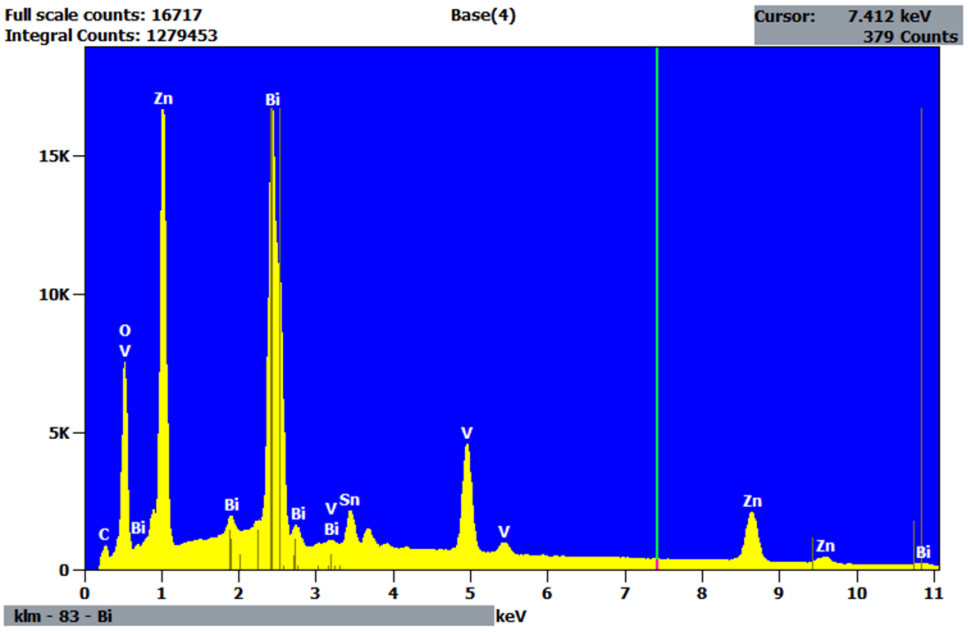

FIGURE 4.6: EDS spectrum of the ZnO/$BiVO_4$ photoanode.

The structure, shown in Fig 4.5 (h), presents the bare FTO surface without any additional coating. A similar structure of FTO was also reported by Keller et al. (2018) [56]. The USP method successfully fabricated ZnO/$BiVO_4$ photoanode and covered the FTO well, as no FTO structure was observed in the other SEM images. Moreover, the energy-dispersive X-ray spectrometer (EDS) spectra of ZnO/$BiVO_4$ are shown in Fig 4.6, which also demonstrates the ZnO/$BiVO_4$ heterojunction was successfully synthesized, because Zn, Bi, and V elements were all homogeneously distributed in the composites. Further, the element's characteristic signal peaks of Zn, Bi and V were observed, and the absence of impurity peaks indicated the photoanode had a high purity and both ZnO and $BiVO_4$ were present.

4.3 Photoelectrochemical and electrochemical properties

4.3.1 LSV and Photocurrent analysis

Linear sweep voltammetry (LSV) curves of the $BiVO_4$ and ZnO/$BiVO_4$ photoanodes were measured at a scan rate of 0.1 V/s in 0.2 M Na_2SO_4 solution under with and without illumination. As shown in Fig 4.7, for both $BiVO_4$ and ZnO/$BiVO_4$ photoanodes, only negligible current was exhibited in the dark condition. In the light condition, the observed current of ZnO/$BiVO_4$ was only higher than $BiVO_4$ photoanode below 0.62 V. From 0.62 V to 1.3 V, the current of $BiVO_4$ photoanode was higher than ZnO/$BiVO_4$ photoanode and kept increasing. However, this finding did not support the previous study that the heterojunction structure could increase the mobility of charge carriers under excitation by solar energy [57].

The photocurrent behaviour was recorded at 1 V potential bias with chopped illumination at 1 s intervals in the spiked real effluent and 0.1 M Na_2SO_4 solution for three hours to investigate the photo-responses of the $BiVO_4$ and ZnO/$BiVO_4$ photoanodes with different cathode materials over time. Fig 4.8 illustrates the reproducible photocurrent with sharp peaks repeatedly ascending and descending under a light on and off cycles, respectively.

At first, a carbon stick was applied as the cathode. The results of the observed photocurrent of $BiVO_4$ and ZnO/$BiVO_4$ photoanodes accorded with previous findings in LSV analysis. As shown in Fig 4.8, all the photocurrent was steady, about 1.2 mA and 0.8 mA for $BiVO_4$ and ZnO/$BiVO_4$ photoanodes, respectively. Next, the carbon stick was replaced with a Pt mesh as the cathode. The observed photocurrent was improved in the first three cycles, then decreased steadily from 2.6 mA to 0.2 mA in the last cycle.

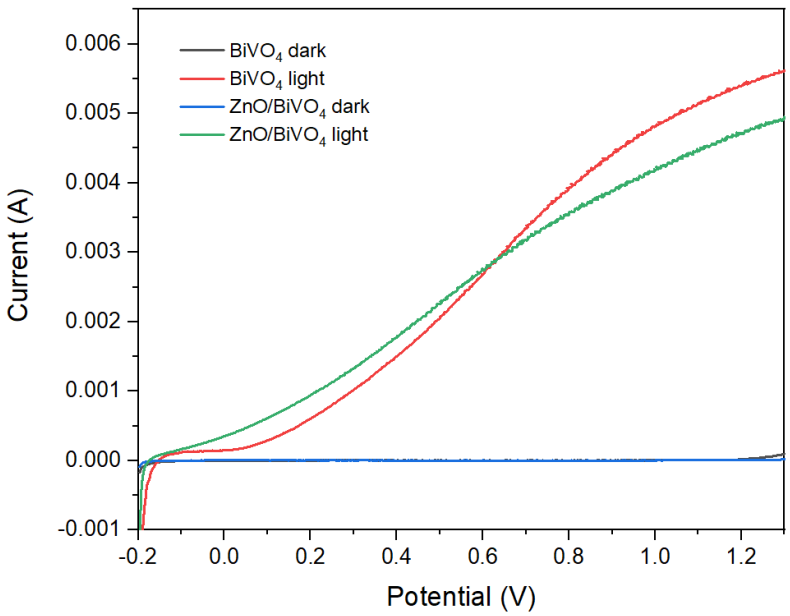

FIGURE 4.7: LSV curves of the $BiVO_4$ and $ZnO/BiVO_4$ photoanodes at a scan rate of 0.1 V/s in dark and light conditions.

However, this result has not previously been described [58, 59]. The reason could be that the tested time was short in the previous study. Therefore, further research should be undertaken to investigate the factors that might influence photocurrent.

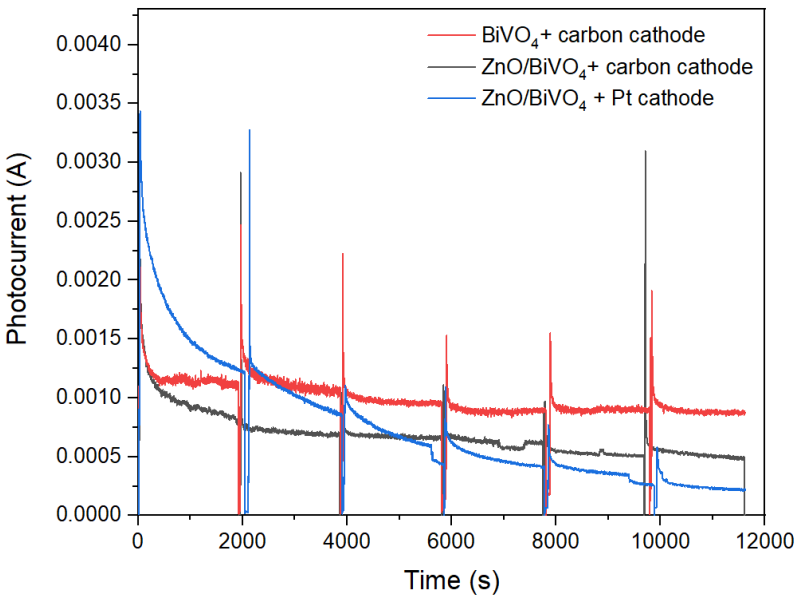

FIGURE 4.8: Photocurrent versus time plots of $BiVO_4$ and $ZnO/BiVO_4$ photoanodes with different cathode materials: Pt mesh and carbon stick which were recorded in the degradation experiments.

4.3.2 EIS analysis

Electrochemical Impedance Spectroscopy (EIS) Nyquist analysis was used to determine the electrochemical behaviours, especially the interfacial charge transfer phenomenon and charge carriers' separation efficiency in the heterojunction. The measurements was carried out in 0.2 M Na_2SO_4 solution at a bias potential of 1 V in both dark and light conditions.

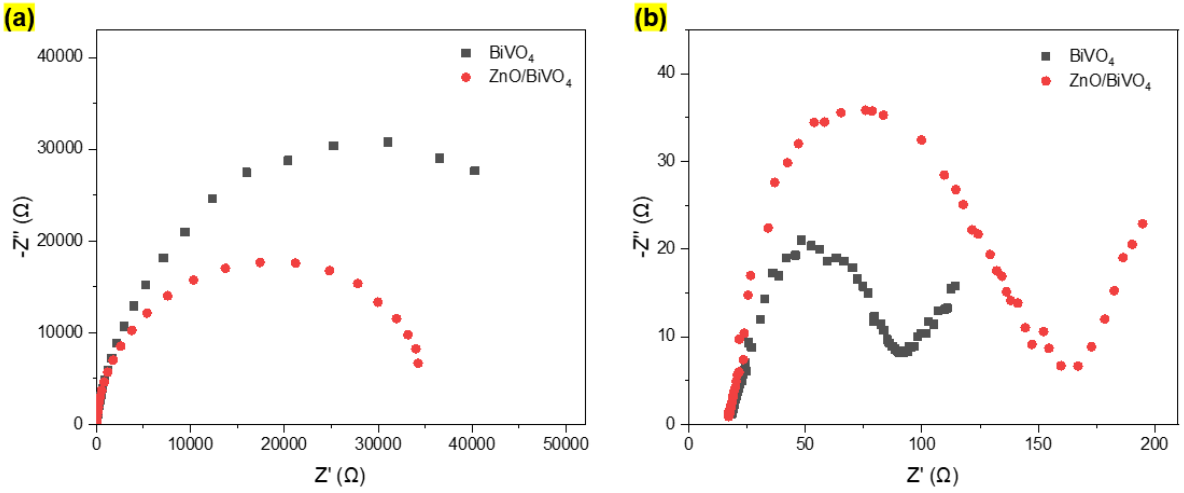

FIGURE 4.9: EIS Nyquist plots for $BiVO_4$ and $ZnO/BiVO_4$ photoanodes in (a) dark, (b) light condition.

As can be seen in Fig 4.9, the observed sense-circular arc presents the charge-transfer resistance (R_{ct}) of $BiVO_4$ and $ZnO/BiVO_4$ photoanodes. Consistent with the literature, the smaller the arc radius indicates, the higher the charge transfer efficiency [47, 60]. Therefore, the observed R_{ct} in dark condition was much higher than the light one. Fig 4.9 (a) illustrates the $BiVO_4$ photoanode had higher R_{ct} than $ZnO/BiVO_4$ photoanode in the dark condition as indicated by the larger semi-circular arc.

The EIS plot in the light condition is shown in Fig 4.9 (b), which includes a semi-circular part and a linear part with a slope of 45 ^{o} belonging to the diffusion-controlled step. The linear part characteristic of the lower frequency is attributable to a diffusional limited electron transfer [61]. The R_{ct} of $BiVO_4$ was lower than the $ZnO/BiVO_4$ photoanode, which previously indicates a more effective separation of photo-induced electron-hole pairs and faster interfacial charge [62]. This finding was in agreement with our LSV results because higher R_{ct} are more likely to have lower photocurrent [63].

In contrast to earlier findings [62, 60], however, the photoanode with the higher R_{ct} achieved higher degradation efficiency in the PEC experiments mentioned in Section 4.6.

This observation may support the explanation that the electrons produced by the photoanode tend to transform into superoxide radical anion ($\cdot O_2^-$) rather than go through the wire to the cathode. In this case, the lower photocurrent and higher R_{ct} were recorded, the higher the degradation efficiency would achieve.

4.4 XPS analysis

The graphene dots (GDs) was doped in the $ZnO/BiVO_4$ to further enhance the PEC process in Section 4.6.3.1. The X-ray photoelectron spectroscopy (XPS) was carried out to determine whether the GD has successfully doped in $ZnO/BiVO_4$ heterojunction. As can be seen in Fig 4.10, the surface composition and chemical states of constituent elements of the $ZnO@GD/BiVO_4$, $ZnO/BiVO_4$, pure $BiVO_4$, pure ZnO and GDs photoanodes were investigated in the binding energy range of 0-1300eV.

Fig 4.10 (a) demonstrates the survey spectrum of each photoanode. Zn 2p, V 2p and Bi 4f can be observed in full spectra. The $ZnO@GD/BiVO_4$ heterojunction was successfully fabricated due to no peaks representing other elements. Zn 2p of $ZnO@GD/BiVO_4$ heterojunction in Fig 4.10 (b) shows the binding energy peaks at 1021.78eV (Zn $2p_{3/2}$) and 1044.88eV (Zn $2p_{1/2}$). The binding energy of each peak in $ZnO@GD/BiVO_4$ was higher than the $ZnO/BiVO_4$. This slight shift of Zn 2p binding energy peaks could be attributed to the strong interfacial interactions between ZnO and GD [64]. The peaks of 530.38 eV and 516.98 eV in Fig 4.10 (d), attributed to the binding energy of V $2P_{2/1}$ and V $2P_{3/2}$ [65]. As can be seen from 4.10 (e), the peaks of 164.18 eV and 158.88 eV can be attributed to Bi $4f_{5/2}$ and Bi $4f_{7/2}$. Therefore, Bi^{3+} existed in the photoanodes [66].

After doping GDs in the $ZnO/BiVO_4$ film, a slight shift can be observed in Fig 4.10 (b-e). The shift to high binding energies may be a result of the facilitation of charge transfer across the $ZnO@GD/BiVO_4$ heterojunction owing to the strong interfacial interactions between the ZnO@GD and $BiVO_4$ in the ternary nanocomposite [67]. A similar shift has already been observed by Wang et al. (2021) [68]. Therefore, the GD was successfully doped in the $ZnO/BiVO_4$ film by the USP method. Moreover, the electronic interaction energy in the ternary heterojunction nanocomposite should enhance charge transfer across hetero-interface, which will support increasing the PEC process [64]. The results of the enhancement to the degradation experiments were described in Section 4.6.3.1.

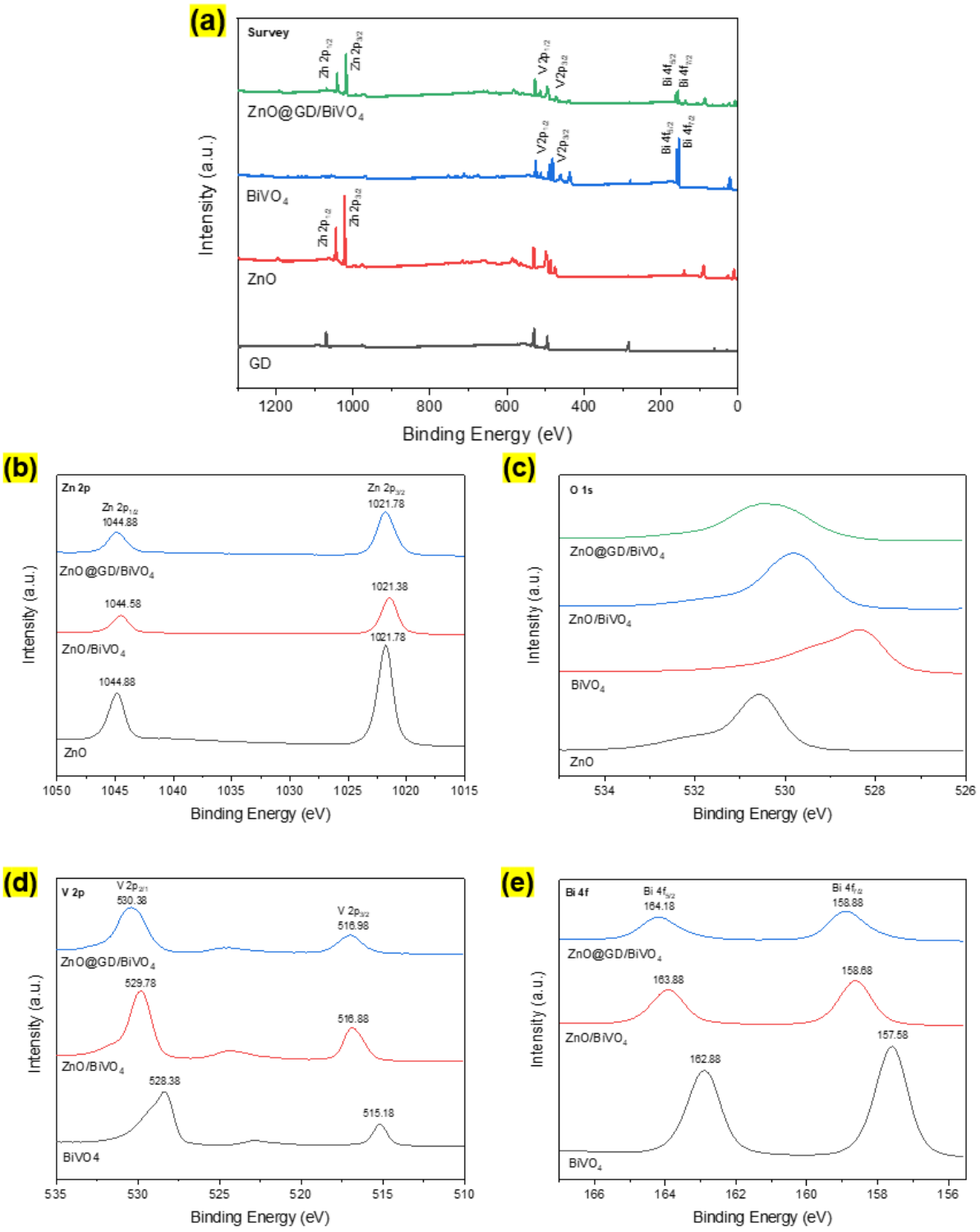

FIGURE 4.10: (a) XPS survey spectra, (b) Zn 2p, (c) O 1s, (d) V 2p, (e) Bi 4f XPS spectra of the ZnO@GD/$BiVO_4$, ZnO/$BiVO_4$, pure $BiVO_4$, pure ZnO and GD photoanodes.

4.5 Optical properties

4.5.1 UV-vis analysis

As shown in Fig 4.11 (a), the UV–vis diffuse reflectance spectra (DRS) were used to analyse pure GDs, pure ZnO, ZnO/GD, ZnO/$BiVO_4$ and ZnO@GD/$BiVO_4$ photoanodes in the wavelength range of 280–650 nm. The wavelength range of the visible spectrum is from 380 to 750 nm [69]. This finding was also reported by Pathak et al. (2018) that the optical bandgap absorption of ZnO was less than 400 nm [70]. However, when doped GD in ZnO film, not only the shift in the absorption edge was observed, and the absorption intensity increased in the range of 280-400 nm. Similar observations to enhance light absorption were previously reported by Kumar et al. [64]. Compared to ZnO with ZnO/$BiVO_4$ heterojunction, there was a larger shift and a higher enhancement of absorption intensity. The sharp band shifted from 400 nm to about 500 nm due to $BiVO_4$ being a visible-light active photocatalyst [60]. Therefore, the ZnO/$BiVO_4$ heterojunction was proven to induce a shift in the absorption spectrum towards the visible-light region for enhanced photo-responsiveness. However, when doped GD into the ZnO/$BiVO_4$ heterojunction, a decrease in absorption intensity was obtained at the spectrum range of 350-480 nm. This result, therefore, needs to be interpreted with caution because it could be an important issue for future research.

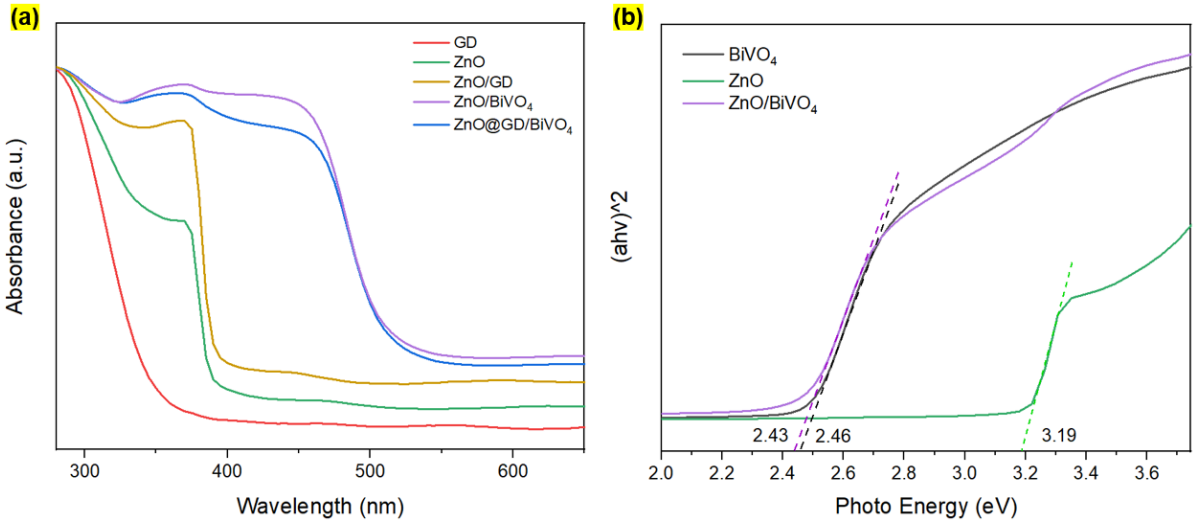

FIGURE 4.11: (a) The UV-vis absorbance spectra of GD, ZnO, ZnO/GD, ZnO/$BiVO_4$ and ZnO@GD/$BiVO_4$, (b) The estimated band gap edges of pure ZnO, pure $BiVO_4$ and ZnO/$BiVO_4$.

Following this, in order to calculate the band gap energies of the crystalline semiconductors, the Tauc approach was first used to estimate the pure ZnO, pure $BiVO_4$ and ZnO/$BiVO_4$ as shown in Equation 4.2 [71], the obtained curves are presented in Fig 4.11 (b):

$$\alpha h\upsilon = A(h\upsilon - E_g)^{n/2} \tag{4.2}$$

Where,
α = absorption coefficient,
$h\upsilon$ = photo energy,
A= proportionality constant,
E_g=band gap (eV),
n = 1 for both BiVO4 and ZnO (n=1 for a direct transition and n=4 for an indirect transition) [59].

Next, extended the tangent lines of the obtained curves in Fig 4.11 (b) to the interception of the x-axis for Tauc's plot to estimate the values of the energy band gap. Fig 4.11 (b) shows the energy band gap values of the pure ZnO, pure $BiVO_4$ and ZnO/$BiVO_4$, of 3.19 eV, 2.48 eV and 2.43 eV, respectively. The ZnO/$BiVO_4$ heterojunction had the lowest energy band gap. And the prior studies that have noted that the narrower band gap is, the better electronic transition and generation of active species are [72]. It also indicated that the ZnO/$BiVO_4$ heterojunction was successfully fabricated.

4.5.2 IPCE analysis

The incident photon-to-current conversion efficiencies (IPCE) for pure ZnO, pure $BiVO_4$ and ZnO/$BiVO_4$ photoanodes were evaluated under the monochromatic light illumination condition in the spiked real effluent and 0.1 M Na_2SO_4 solution at 1 V potential bias. The wavelength-dependent IPCE calculations were carried out by Equation 4.3 [73]:

$$IPCE(\%) = \frac{I_{ph}(A)}{P(W)} \times \frac{1240}{\lambda(nm)} = \frac{Electrons/sec}{Photons/sec} \times 100 \tag{4.3}$$

Where,
I_{ph} = photocurrent,
λ = wavenumber of the monochromatic light,
P = power density of the light source.

Fig 4.12 revealed the contribution of photoanodes optical properties by the heterojunction of ZnO/$BiVO_4$. The IPCE result of the ZnO photoanode accorded to the previous DRS result that the electrons were unable to be created under visible light. However, the $BiVO_4$ had higher IPCE than ZnO/$BiVO_4$ photoanode of 21.5 % at 350 nm and 3.8 % at 365 nm, respectively and a similar wavelength range. Although the IPCE results accorded to our LSV and EIS results, they were contrary to previous studies which have suggested that the photoanodes with higher IPCE results would have higher degradation efficiencies [74, 75]. As the explanation mentioned in Section 4.3.2, most of the created electrons may have been transformed into superoxide radical anion and went into the solution except for the wire, which might also explain the IPCE results. Future studies on the current phenomenon are therefore recommended.

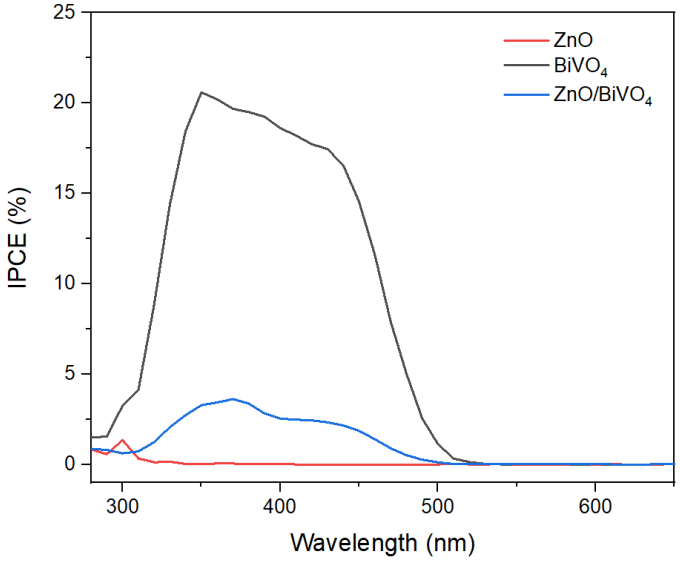

FIGURE 4.12: IPCE plot under monochromatic irradiation for pristine pure ZnO, pure $BiVO_4$ and ZnO/$BiVO_4$ photoanodes.

4.6 PEC Degradation Experiments

Fig 4.13 illustrates the mechanism of the PEC degradation experiment. The ZnO@GD/$BiVO_4$ photoanode was placed under the simulated solar irradiation and at 1 V potential bias in a 147 mL different water sample with 0.1 M Na_2SO_4. Then, as Equation 4.4-4.6 shows, the generated electrons and holes would react with the O_2 and H_2O to create ($\cdot O_2^-$) superoxide radical anion and ($\cdot OH$) hydroxyl radicals, respectively. At last, the radicals would degrade the target OMPs in the solution. The Netherlands standard of OMPs total removal efficiency is seven of 11 OMPs achieve more than 70% (ISBN 978.90.5773.874.6, STOWA,

2020).

$$Absorption\ of\ solarenergy : Semi - conductor + h\nu(> E_g) = e^- + h^+ \tag{4.4}$$

$$\cdot OH\ production : H_2O + h^+ = H^+ + \cdot OH \tag{4.5}$$

$$\cdot O_2^-\ production : e^- + O_2 = \cdot O_2^- \tag{4.6}$$

Therefore, the following experiments would start from degraded OMPs in MiliQ, then degraded OMPs in real WWTPs effluent. The concentration of TOC and COD would be measured to analyse whether they interfere with the degradation or not. Further, the PEC process was enhanced in two different approaches: (1) GDs were doped in the ZnO/$BiVO_4$ photoanodes, and (2) persulfate was added to the solution.

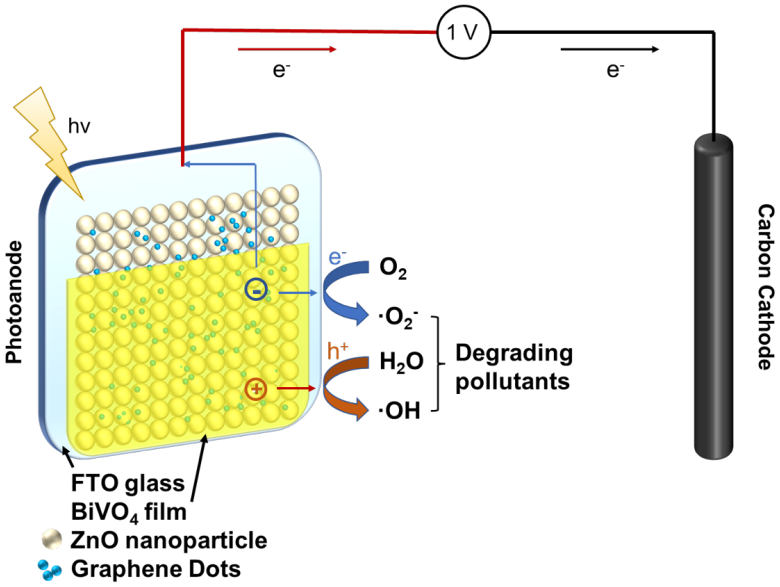

FIGURE 4.13: The mechanism of the PEC degradation experiments.

4.6.1 PEC Degradation Experiments in Spiked MiliQ

The ZnO/$BiVO_4$ photoanode was applied to remove 10 μg/L 11 OMPs in spiked MiliQ solution by solar-driven PEC degradation. The removal of 11 OMPs were observed through the LC-MS through the formation of intermediate products corresponding to new peaks in the chromatograms. As shown in Fig 4.14, after three hours PEC process, nine of 11 OMPs had more than 70 % total degradation efficiency, which met the Netherlands standard.

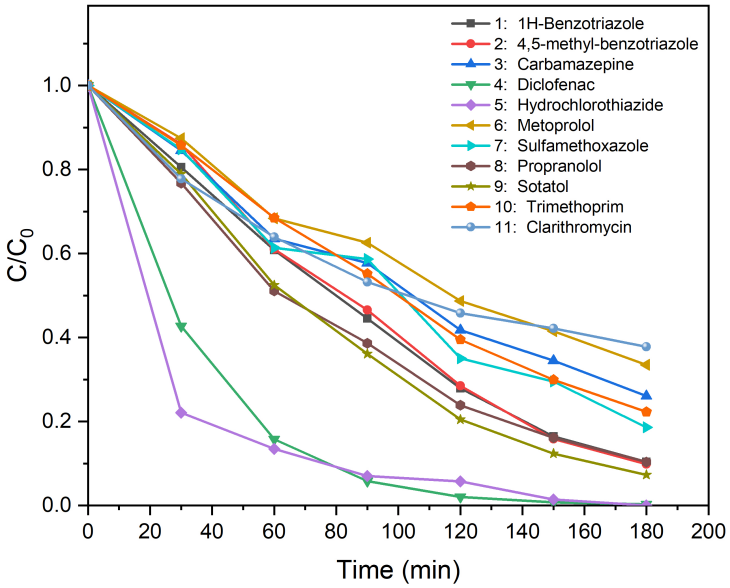

FIGURE 4.14: Normalised concentration versus time plot for PEC degradation of 11 OMPs on $ZnO/BiVO_4$ photoanode in spiked MiliQ.

Table 4.1 shows that only MP and CLA did not achieve 70 %, of 66.50 % and 62.19 % total degradation efficiency, respectively. The DIC and HCTZ had the highest degradation efficiency, of 99% in three hours PEC process. The BAT, MBTA, PRO and SOT had about 90 % degradation efficiency. A pseudo-first-order kinetic model ($C/C_0=e^{-kt}$) is fitted to measurements (i.e. degradation efficiencies) of each 11 OMPs and plotted into the Fig 4.16. The kinetic rate coefficient (k) obtained are shown in Table 4.1. The highest k of 43.62×10^{-3} min^{-1} was for HCTZ degradation. However, the lowest k of 7.00×10^{-3} min^{-1} was obtained from the degradation of CBZ.

4.6.2 PEC Degradation Experiments in Real WWTPs Effluent

Because the $ZnO/BiVO_4$ photoanode was successfully applied to the spiked MiliQ degradation and met the standard. Next, in this section, the degradation experiments were carried out in 10 μg/L spiked real WWTPs effluent at 1 V potential bias under solar-driven PEC process. Both $BiVO_4$ and $ZnO/BiVO_4$ photoanodes were applied to the degradation and the degradation efficiencies were compared.

As shown in Fig 4.15, only DIC, HCTZ, PRO and SOT achieved more than 70% degradation efficiency, which did not meet the Netherlands standard. The total degradation

TABLE 4.1: The total degradation efficiency (TD) and fitted kinetics coefficient for the PEC degradation of $BiVO_4$ and $ZnO/BiVO_4$ in spiked real effluent and $ZnO/BiVO_4$ in spiked MiliQ.

OMPs	$BiVO_4$ in spiked effluent	$ZnO/BiVO_4$ in spiked effluent		$ZnO/BiVO_4$ in spiked MiliQ	
Name	TD (%)	TD (%)	k ($\times 10^{-3}$ min^{-1})	TD (%)	k ($\times 10^{-3}$ min^{-1})
1. BTA	12.44	52.31	4.77	89.59	9.96
2. MBTA	26.65	53.45	5.06	90.16	9.70
3. CBZ	25.04	46.22	4.17	73.93	7.00
4. DIC	99.42	99.76	34.44	99.74	29.71
5. HCTZ	98.94	100.00	29.86	100.00	43.62
6. MP	19.67	41.99	3.68	66.50	5.82
7. SMX	25.45	61.54	5.22	81.38	7.83
8. PRO	84.54	91.02	13.64	89.63	11.25
9. SOT	85.43	91.39	12.39	92.71	11.81
10. TMP	21.25	55.88	5.11	77.71	7.35
11. CLA	61.04	49.48	2.66	62.19	6.33

efficiency of DIC and HCTZ also reached 99% in three hours PEC process. The other two OMPs with more than 70% degradation efficiency were PRO and SOT, with about 90%. The rest seven OMPs did not meet the standard and had about 55% degradation efficiency on average. As can be seen in Table 4.1, compared to the total degradation efficiencies in spiked MiliQ, all the efficiencies showed a decrease except DIC and HCTZ. To further explore the details of the differences between the degradation in spiked MiliQ and real effluent water, the normalised concentration and fitted kinetic curves were plotted in Fig 4.16 for each OMP.

As shown in Fig 4.16, the $ZnO/BiVO_4$ had higher degradation efficiency than $BiVO_4$ photoanode for most of OMPs, which means the $ZnO/BiVO_4$ heterojunction was successfully fabricated and was able to enhance the PEC process. As for DIC, almost no difference was shown between the degradation efficiency of the three conditions, and the kinetic coefficients were high.

Compared to the degradation in spiked MiliQ, the degradation efficiency of BTA, MBTA, CBZ, HCTZ, MP, SMX, TMP, and CLA decreased. Therefore, the real WWTPs effluents were observed to inhibit the OMPs degradation process. For PRO and SOT, it presented a less inhibition effect. The k value in spiked real effluent degradation in Table 4.1 also presents the inhibition effect. As for HCTZ, the k value decreased from 43.62×10^{-3} min^{-1} to 29.86×10^{-3} min^{-1} in spiked real effluent degradation, which had the highest

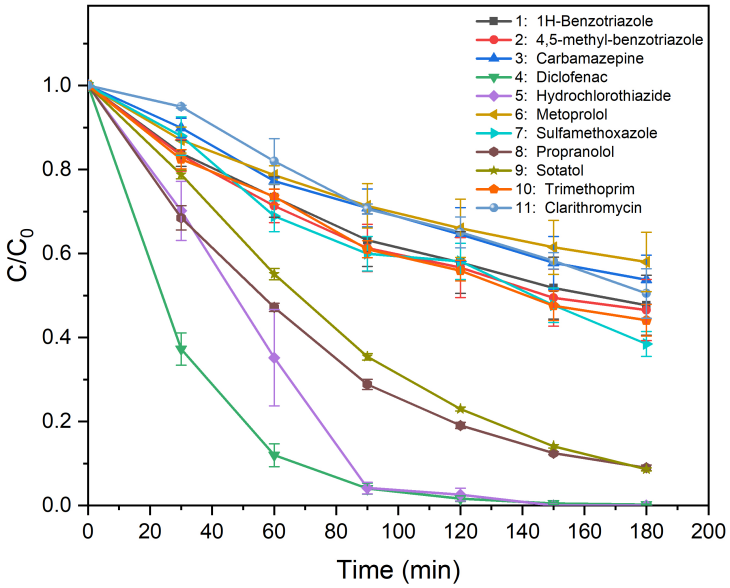

FIGURE 4.15: Normalised concentration versus time plot for PEC degradation of 11 OMPs on $ZnO/BiVO_4$ photoanode in spiked real WWTPs effluent.

inhibition effect. Other OMPs had reduced about 3×10^{-3} min^{-1}, such as CBZ reduced from 7.00×10^{-3} min^{-1} to 4.17×10^{-3} min^{-1}.

4.6.3 Other Pollutants Analysis

The results of other common pollutants are shown in Table 4.2 for the degradation experiments in spiked MiliQ. After three hours of the PEC process, the TOC increased from 0.83 mg/L to 3.04 mg/L, which was contrary to the results found by Sousa et al. (2012)[76], that the TOC should decrease because of the mineralization of OMPs. Moreover, the concentrations of COD and NO_3-N also increased. The pH of the solution was decreased as the result of the ·OH production in Equation 4.5.

TABLE 4.2: Concentrations of other common pollutants before and after degradation experiments in spiked MiliQ.

Sample Name	TOC mg/L	COD mg/L	NO_3-N mg/L	pH a.u.
Spiked MiliQ	0.83	-	0.09	7.26
Spiked MiliQ after degradation	3.04	10.44	0.16	6.82

'-' means under detection range.

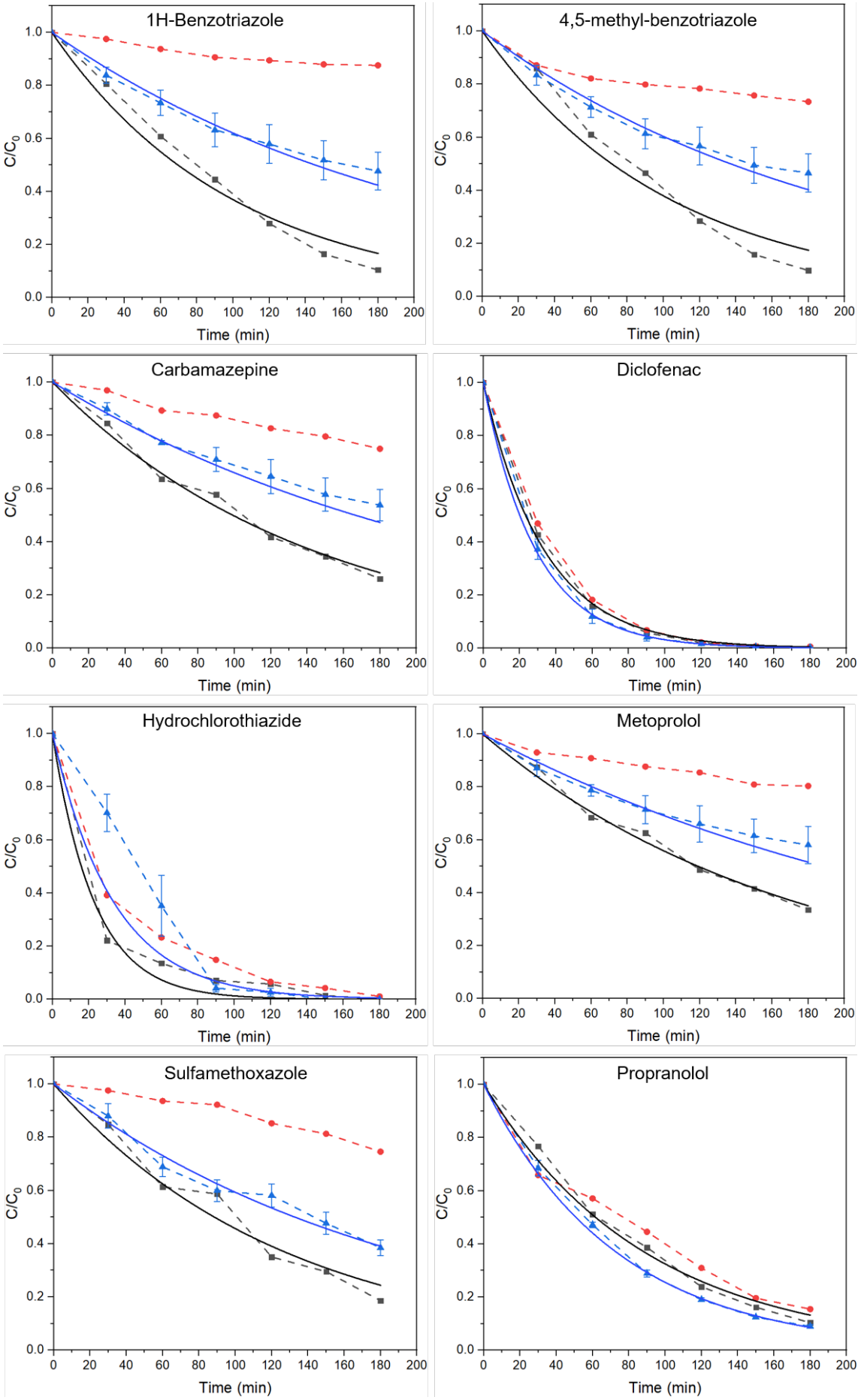
1H-Benzotriazole
4,5-methyl-benzotriazole
Carbamazepine
Diclofenac
Hydrochlorothiazide
Metoprolol
Sulfamethoxazole
Propranolol
C/C0
Time (min)
0.0
0.2
0.4
0.6
0.8
1.0
0
20
40
60
80
100
120
140
160
180
200

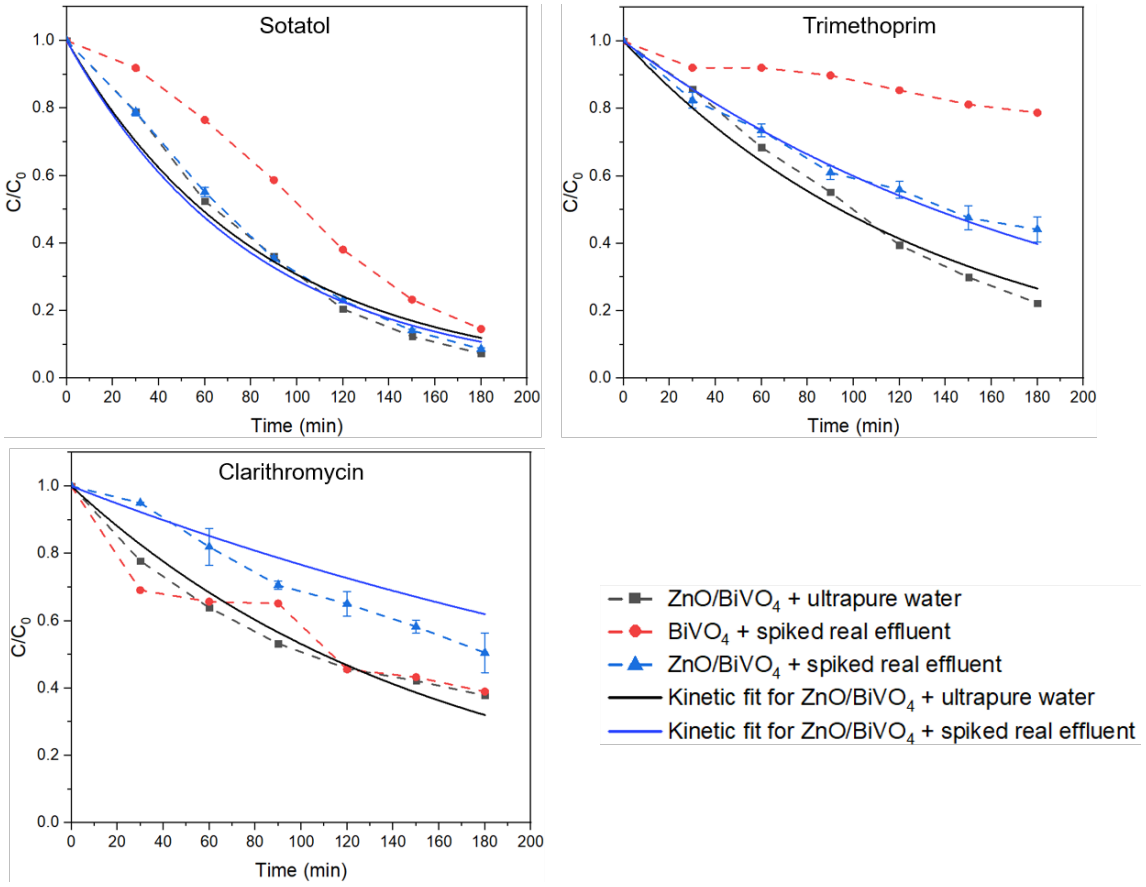

FIGURE 4.16: Normalised concentration versus time and fitted kinetic curve for PEC degradation of 11 OMPs on $BiVO_4$ and $ZnO/BiVO_4$ photoanode in spiked real WWTPs effluent, $ZnO/BiVO_4$ photoanode in spiked MiliQ.

TABLE 4.3: Concentrations of other common pollutants in the solution of before and after degradation experiments in real WWTPs effluent.

Sample Name	TOC mg/L	COD mg/L	NO_3-N mg/L	pH a.u.
Origin effluent	11.11	31.8	1.63	7.74
Spiked effluent	11.60	32.5	1.88	8.13
Spiked effluent after $BiVO_4$ degradation	12.66	37.5	2.42	8.02
Spiked effluent after $ZnO/BiVO_4$ degradation	12.74	38.7	2.45	7.69

Next, the concentrations of other pollutants were measured before and after the degradation in real WWTPs effluents to further study the PEC process. The results are presented in Table 4.3. After spiking the filtered effluent with 10 μg/L 11 OMPs, the TOC and COD had a slight increase due to the OMPs also contributing to the measured values. After three hours of the PEC process, the concentrations of TOC, COD and NO_3-N increased for both $BiVO_4$ and $ZnO/BiVO_4$ photoanodes. The reason for the NO_3-N increase might be the NO_2-N in the origin effluent was oxidized by radicals. However, the finding of COD and TOC increase is contrary to previous studies, which have suggested that COD and TOC should decrease due to the OMPs mineralized to CO_2 and H_2O in the PEC process [77]. This inconsistency may be due to two reasons. First, the OMPs are hard to be degraded. They could not be split into smaller molecules or be mineralized to CO_2 and H_2O in three hours of PEC process [78]. Second, the carbon stick cathode could be damaged by the radicals. Then the tiny carbon pieces caused the increase in COD and TOC.

Moreover, the $ZnO/BiVO_4$ heterojunction had a higher amount of TOC and COD growth than $BiVO_4$. It can thus be suggested that the $ZnO/BiVO_4$ heterojunction could create more radicals and cause more damage to the carbon stick cathode. However, the OMPs were probably split into non-toxic, biodegradable, smaller molecules. In this case, it could be further treated by the biodegradation process as a combined post-treatment.

Table 4.4: Concentrations of other common pollutants in the solution of before and after degradation experiments in real WWTPs effluent with carbon stick and Pt mesh cathode.

Sample Name	TOC mg/L	COD mg/L	NO_3-N mg/L	pH a.u.
Origin spiked effluent	11.99	32.5	1.88	8.13
Degraded spiked effluent with carbon stick cathode	12.74	38.7	2.45	7.69
Degraded spiked effluent with Pt mesh cathode	11.92	30.2	2.26	7.74

In order to eliminate the effect of the carbon stick cathode, the cathode was replaced with a Pt mesh for the PEC degradation experiment. As can be seen in Table 4.4, the concentrations of TOC and COD decreased after the degradation when applied Pt mesh as the cathode. This result indicated that the organic carbon observed in the previously increased fraction of TOC came from the carbon stick cathode. However, the increase of COD concentration was because of the contamination of carbon sticks. As the previous study suggested that the carbon stick is capable to absorb OMPs [79]. This means that the carbon stick was not completely cleaned at the end of the previous experiments.

Simultaneously, it also indicated that the PEC process could cause damage to the carbon stick cathode.

4.6.4 Enhanced PEC Degradation Experiments in Real WWTPs Effluent

When $ZnO/BiVO_4$ photoanode was applied in real WWTPs effluent treatment, only four of 11 OMPs achieved more than 70 % degradation efficiency in three hours PEC process, which did not meet the standard in the Netherlands. Consequently, three more approaches were tested in this section to enhance the PEC process and increase the degradation efficiency during the same degradation period.

4.6.4.1 Doped GD

As mentioned in the literature review, Graphene Dots (GDs) have two main benefits for enhancing the PEC process. It first can be attributed to the extended light absorption in the visible spectrum region, which was also accorded to the results in Section 4.5.1 and presented in Fig 4.11 (a). Therefore, GDs are able to enhance electron-holes separation efficiency remarkably. Simultaneously, the photogenerated electrons are trapped by GDs. Then, GDs can enhance effective in-situ production of superoxide radicals ($\cdot O_2^-$) from captured O_2 in the reaction systems, which can further oxidize the OMPs [38].

2 % GD had been doped to the ZnO paste and the $ZnO@GD/BiVO_4$ photoanode has been prepared by the USP method. The XPS results in Section 4.4 and Fig 4.10 illustrate that the GD had been successfully doped into the $ZnO/BiVO_4$ heterojunction.The solar-driven PEC degradation experiment was carried out in the spiked real WWTPs effluent with 10 μg/L 11 OMPs and 0.1 M Na_2SO_4 at 1 V potential bias.

Fig 4.17 presents the degradation efficiency for 11 OMPs in the three hours PEC process. The degradation of BAT, MBTA, MP, SOT and CLA increased. Especially for BAT and MBTA, the total degradation efficiency increased from 52.31 % and 53.45 % to 70.98 % and 91.99 %, respectively. For MP, SOT and CLA, the degradation efficiency increased by less than 10 %. For the other OMPs, it presented no significant increase. For instance, the DIC and HCTZ still achieved 100 % degradation efficiency in three hours PEC process. However, despite the fact that the degradation efficiency had increased because of the

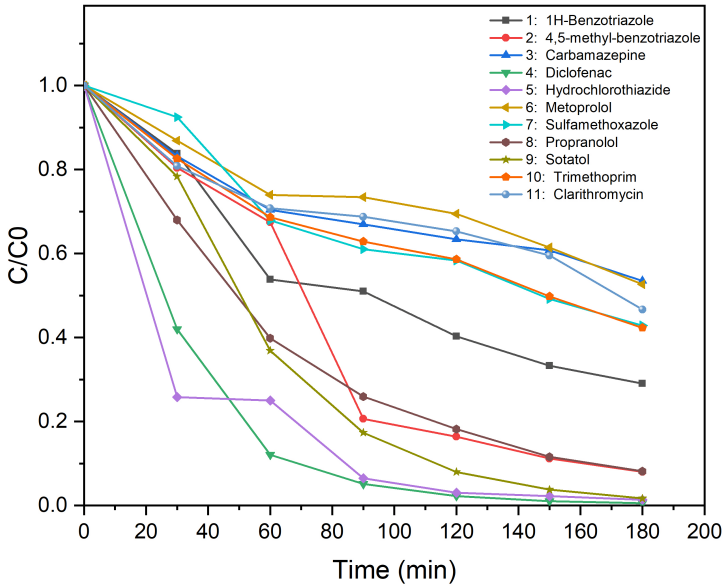

FIGURE 4.17: Normalised concentration decay versus time plot for PEC degradation of 11 OMPs on ZnO@GD/$BiVO_4$ photoanode in spiked real WWTPs effluent.

enhancement by the doped GD, only five of 11 OMPs achieved more than 70 % degradation efficiency. Still, the application of ZnO@GD/$BiVO_4$ photoanode could not meet the Netherlands standard within three hours PEC process.

This observation may support the explanation mentioned in Section 4.3.2 about the EIS results, that the electrons transformed into $\cdot O_2^-$ in the PEC process. Further, prior studies have noted that GD could enhance effective in-situ production of $\cdot O_2^-$. As a result of this, the reason could be that the $\cdot O_2^-$ was the main active species in this study. However, different OMPs might be sensitive to different active species and is easier degraded by one special radical [21]. Therefore, BAT and MBTA were more likely to be degraded by $\cdot O_2^-$. The trapping experiments were therefore carried out to study the effect of different radicals. 5 mM p-benzoquinone and methanol were added to the electrolytic solution to suppress the impact of $\cdot O_2^-$ and $\cdot OH$, respectively, which can be seen in Appendix A.

4.6.4.2 Added Persulfate

The other approach to increase the degradation efficiency is the addition of sulfate radical ($\cdot SO_4^-$). Because the PEC process happened in the area close to the photoanode surface, the OMPs in the bulk solution could be degraded by the free $\cdot SO_4^-$. To obtain the

$\cdot SO_4^-$, sodium persulfate (PS, $S_20_8^{2-}$) need to be activated by physical method [80]. This experiment activated PS by heating, UV irradiation, and metal oxide.

This study added 1 mM PS to the spiked real effluent for PEC degradation (the PS/OMPs molar ratio was above 10:1 [78]). Fig 4.18 illustrates every 11 OMPs degradation with and without PS addition in 60 minutes PEC process. For the first 5 min, the reactor was in dark condition, and no external voltage was applied. Compared to the degradation efficiency of $ZnO/BiVO_4$ photoanode, it shows a decrease for every 11 OMPs, which means the addition of PS could degrade OMPs itself without the PEC process. After starting the PEC process, only HCTZ, SMX, PRO and CLA present a significant increase in degradation efficiency. Further, the $\cdot SO_4^-$ could enhance the degradation of HCTZ, SMX, PRO and CLA. These results provide further support for the hypothesis that different OMPs might be sensitive to a specific radical.

In summary, these two approaches could both enhance the PEC process and increase the degradation efficiency. However, none of them met the standard in the Netherlands.

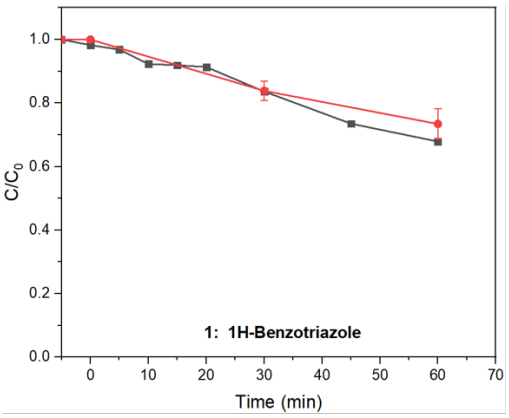
1: 1H-Benzotriazole
C/C0
Time (min)

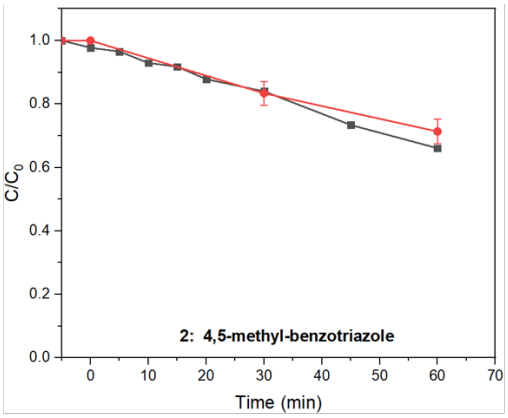
2: 4,5-methyl-benzotriazole
C/C0
Time (min)

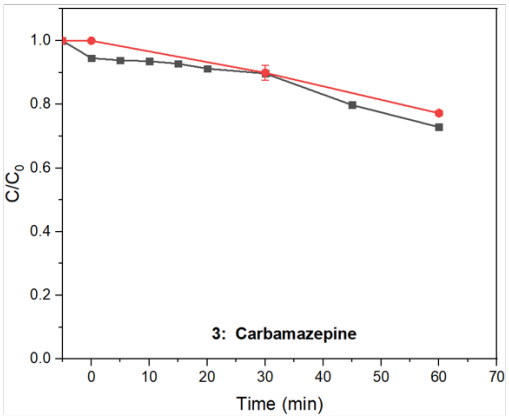
3: Carbamazepine
C/C0
Time (min)

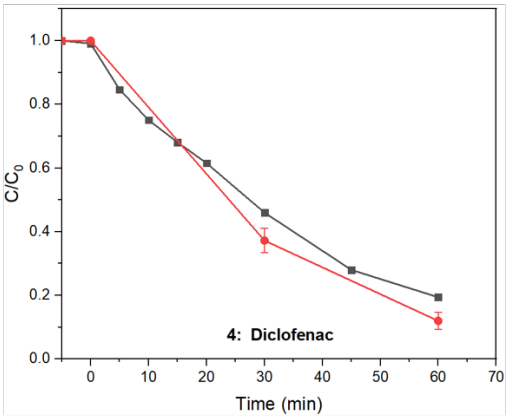
4: Diclofenac
C/C0
Time (min)

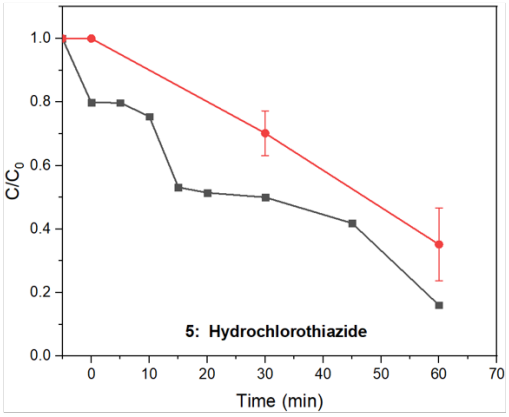
5: Hydrochlorothiazide
C/C0
Time (min)

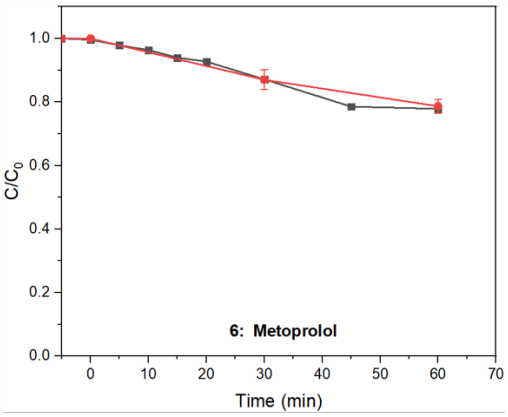
6: Metoprolol
C/C0
Time (min)

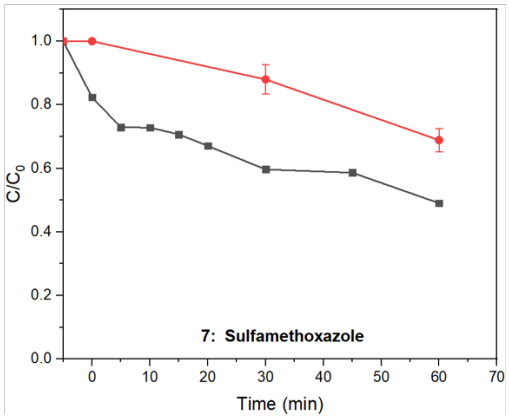
7: Sulfamethoxazole
C/C0
Time (min)

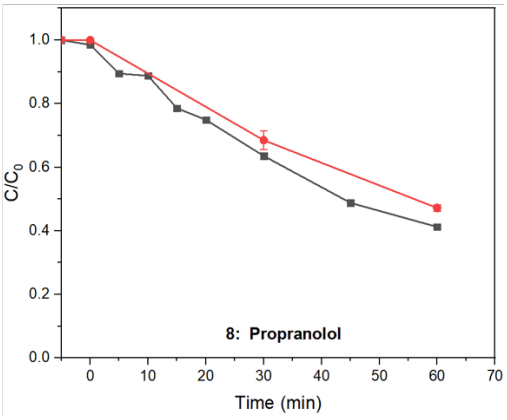
8: Propranolol
C/C0
Time (min)

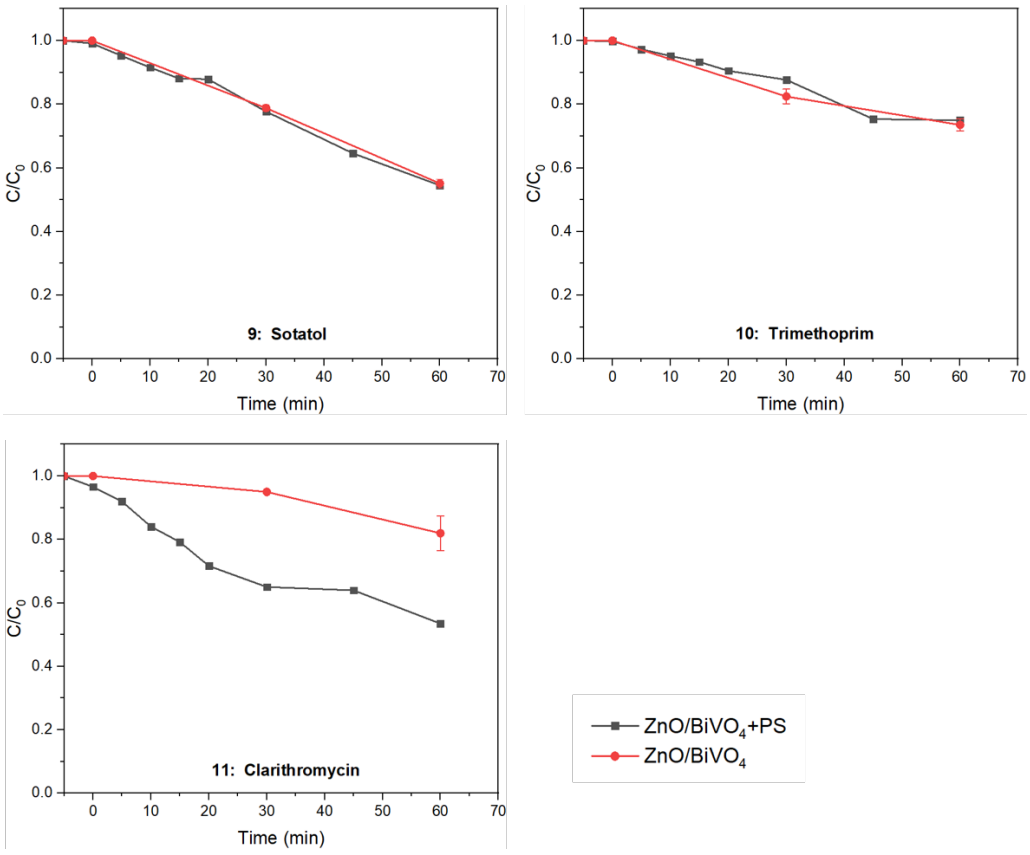

FIGURE 4.18: Normalised concentration decay versus time for PEC degradation of 11 OMPs on $ZnO/BiVO_4$ photoanode in spiked real WWTPs effluent with and without PS addition.

Chapter 5

Conclusions

The first purpose of the study was to fabricate a $ZnO/BiVO_4$ photoanode, that can be applied to WWTPs effluent treatment by a solar-driven PEC process. The second purpose of this study was to investigate the degradation efficiency of selected 11 OMPs using the prepared $ZnO/BiVO_4$ photoanode. Based on the two main parts of the experiments, the proposed research questions can be answered:

1. **What is the proper method to fabricate a photoanode with a heterojunction structure using graphene dots, ZnO and $BiVO_4$? What is the optimal fabrication sequence?**

- The ultrasonic spray pyrolysis was the proper method to conveniently and successfully fabricate $ZnO/BiVO_4$ and ZnO@GD/$BiVO_4$ heterojunction structures. The ZnO(bottom)/$BiVO_4$(top) was the optimal fabrication sequence. The prepared photoanode was semi-transparent, stable and uniform and had high degradation efficiency.

2. **What is the effect of real WWTPs effluent on the degradation efficiency of 11 OMPs for the PEC process?**

- In three hours of solar-driven PEC process, nine of 11 OMPs had achieved more than 70 % degradation efficiency when the $ZnO/BiVO_4$ photoanode was applied to degrade the OMPs in the spiked MiliQ. Only MP and CLA showed less than 70 % but still more than 60 % degradation efficiency. Four of 11 OMPs had observed more than 70 % degradation efficiency when the $ZnO/BiVO_4$ photoanode was applied to degrade the OMPs in the spiked real WWTPs effluent. Except for DIC and SOT,

the degradation efficiencies of other OMPs all presented a decrease. The results of this investigation suggest that the real WWTP effluent had an inhibition effect on the PEC process and reduced the degradation efficiencies of OMPs.

3. **What is the degradation behaviour of other pollutants in PEC process in real WWTP effluent?**

- After three hours of the PEC process, the concentrations of TOC, COD and NO_3-N increased. The increase in TOC and COD was found to be related to the disintegration of the carbon stick cathode.

4. **How to further enhance the PEC process and improve the 11 OMPs degradation efficiency in real WWTPs effluents?**

- This study doped 2 % graphene dots (GDs) in ZnO film and fabricated ZnO@GD/$BiVO_4$ photoanode. The results of UV-vis analysis and PEC degradation experiments confirmed that GDs extended light absorption in the visible spectrum region and increased the degradation efficiency. Five of the 11 OMPs achieved more than 70 % degradation efficiency in three hours of the PEC process. The degradation efficiency of BAT and MBTA had a higher improvement over other OMPs. After doped GDs to the photoanode, the degradation efficiencies of BAT and MBTA increased from 52.31 % to 70.98 % and 53.45 % to 91.99 %, respectively.

- The investigation of persulfate addition has shown that it improved the degradation efficiency by degraded OMPs in bulk solution. The degradation efficiency of HCTZ, SMX, PRO and CLA had a significant improvement over other OMPs by the effect of PS addition. The molar ratio PS: OMPs of 10:1 was determined insufficient for the degradation in spiked real WWTP effluent.

Chapter 6

Limitations and Recommendations

6.1 Limitations

The methods employed in this study had several limitations that should be clarified:

1. The reactor used in the degradation experiments only has one single cell. Therefore, the cathode can influence the degradation performance of the photoanode.
2. The OMPs had low concentration. The concentrations of TOC and COD were under the detection range. Therefore, the results cannot tell whether the OMPs were completely mineralized.
3. Lack of techniques to detect transformation products (TPs) after the PEC process.

6.2 Recommendations

These findings provide the following insights for future research:

1. Further research needs to examine the relationships between the photoelectrochemical properties and OMP degradation efficiency more closely.
2. There were several active species in this study, such as $\cdot O_2^-$, $\cdot OH$ and $\cdot SO_4^-$. The trapping experiments should be carried out to determine whether the radicals could selectively oxidise the OMPs.

3. In order to further enhance the PEC process and meet the OMPs removal standard in the Netherlands, the molar ratio of doped GDs and the weight ratio of added PS should be adjusted to an optimal value.

4. More broadly, research is also needed to determine the composition and toxicity of transformation products (TPs) produced by the PEC process. Also, the PEC process should be further enhanced to mineralise the OMPs to CO_2 and H_2O. Or added post-treatments such as activated carbon and membrane filtration, in order to remove the TPs.

5. Most PEC degradation processes are currently carried out on a lab scale. Further research could explore scaling up the PEC treatment to a pilot scale, which might give more suggestions for the industrial application.

6. The reactor design should be improved to decrease the reaction time. Proton exchange membranes should be used to separate the cathode from the photoanode reaction.

Bibliography

[1] S. McMichael, P. Fernández-Ibáñez, and J. A. Byrne, "A review of photoelectrocatalytic reactors for water and wastewater treatment," *Water*, vol. 13, no. 9, p. 1198, 2021.

[2] N. Noor, "Microplasmas in ZnO nano-forests under high voltage stress," 2019.

[3] M. T. van Vliet, E. R. Jones, M. Flörke, W. H. Franssen, N. Hanasaki, Y. Wada, and J. R. Yearsley, "Global water scarcity including surface water quality and expansions of clean water technologies," *Environmental Research Letters*, vol. 16, no. 2, p. 024020, 2021.

[4] P. Chowdhary, R. N. Bharagava, S. Mishra, and N. Khan, "Role of industries in water scarcity and its adverse effects on environment and human health," in *Environmental concerns and sustainable development*, pp. 235–256, Springer, 2020.

[5] S. Choi, H. Yoom, H. Son, C. Seo, K. Kim, Y. Lee, and Y. M. Kim, "Removal efficiency of organic micropollutants in successive wastewater treatment steps in a full-scale wastewater treatment plant: Bench-scale application of tertiary treatment processes to improve removal of organic micropollutants persisting after secondary treatment," *Chemosphere*, vol. 288, p. 132629, 2022.

[6] A. Govaerts, V. Verhaert, A. Covaci, V. L. Jaspers, O. K. Berg, A. Addo-Bediako, A. Jooste, and L. Bervoets, "Distribution and bioaccumulation of POPs and mercury in the Ga-Selati River (South Africa) and the rivers gudbrandsdalslågen and rena (norway)," *Environment international*, vol. 121, pp. 1319–1330, 2018.

[7] Z. Zhao, X. Yao, Q. Ding, X. Gong, J. Wang, S. Tahir, I. A. Kimirei, and L. Zhang, "A comprehensive evaluation of organic micropollutants (OMPs) pollution and prioritization in equatorial lakes from mainland Tanzania, East Africa," *Water Research*, vol. 217, p. 118400, 2022.

[8] D. Bertagna Silva, G. Buttiglieri, and S. Babić, "State-of-the-art and current challenges for TiO2/UV-LED photocatalytic degradation of emerging organic micropollutants," *Environmental Science and Pollution Research*, vol. 28, no. 1, pp. 103–120, 2021.

[9] R. Wang, M. Ji, H. Zhai, Y. Guo, and Y. Liu, "Occurrence of antibiotics and antibiotic resistance genes in WWTP effluent-receiving water bodies and reclaimed wastewater treatment plants," *Science of The Total Environment*, vol. 796, p. 148919, 2021.

[10] T. C. Schmidt, "Recent trends in water analysis triggering future monitoring of organic micropollutants," *Analytical and bioanalytical chemistry*, vol. 410, no. 17, pp. 3933–3941, 2018.

[11] A. Jurado, M. Walther, and M. S. Díaz-Cruz, "Occurrence, fate and environmental risk assessment of the organic microcontaminants included in the watch lists set by EU decisions 2015/495 and 2018/840 in the groundwater of Spain," *Science of the Total Environment*, vol. 663, pp. 285–296, 2019.

[12] R. Loos, R. Carvalho, D. C. António, S. Comero, G. Locoro, S. Tavazzi, B. Paracchini, M. Ghiani, T. Lettieri, L. Blaha, *et al.*, "EU-wide monitoring survey on emerging polar organic contaminants in wastewater treatment plant effluents," *Water research*, vol. 47, no. 17, pp. 6475–6487, 2013.

[13] R. Guillossou, J. Le Roux, R. Mailler, E. Vulliet, C. Morlay, F. Nauleau, J. Gasperi, and V. Rocher, "Organic micropollutants in a large wastewater treatment plant: what are the benefits of an advanced treatment by activated carbon adsorption in comparison to conventional treatment," *Chemosphere*, vol. 218, pp. 1050–1060, 2019.

[14] S. Arriaga, N. de Jonge, M. L. Nielsen, H. R. Andersen, V. Borregaard, K. Jewel, T. A. Ternes, and J. L. Nielsen, "Evaluation of a membrane bioreactor system as post-treatment in waste water treatment for better removal of micropollutants," *Water research*, vol. 107, pp. 37–46, 2016.

[15] S. Ahmed, M. Rasul, W. N. Martens, R. Brown, and M. Hashib, "Advances in heterogeneous photocatalytic degradation of phenols and dyes in wastewater: a review," *Water, Air, & Soil Pollution*, vol. 215, no. 1, pp. 3–29, 2011.

[16] Z. Zhang, X. Li, Z. Ma, H. Ning, D. Zhang, and Y. Wang, "A facile and green strategy to simultaneously enhance the flame retardant and mechanical properties of poly (vinyl alcohol) by introduction of a bio-based polyelectrolyte complex formed

by chitosan and phytic acid," *Dalton Transactions*, vol. 49, no. 32, pp. 11226–11237, 2020.

[17] B. O. Orimolade and O. A. Arotiba, "Bismuth vanadate in photoelectrocatalytic water treatment systems for the degradation of organics: A review on recent trends," *Journal of Electroanalytical Chemistry*, vol. 878, p. 114724, 2020.

[18] M. Tayebi, M. Kolaei, A. Tayyebi, Z. Masoumi, Z. Belbasi, and B.-K. Lee, "Reduced graphene oxide (RGO) on TiO2 for an improved photoelectrochemical (PEC) and photocatalytic activity," *Solar Energy*, vol. 190, pp. 185–194, 2019.

[19] D. Cao, Y. Wang, and X. Zhao, "Combination of photocatalytic and electrochemical degradation of organic pollutants from water," *Current Opinion in Green and Sustainable Chemistry*, vol. 6, pp. 78–84, 2017.

[20] W. Tang, Y. Zhang, J. Bai, J. Li, J. Wang, L. Li, T. Zhou, S. Chen, M. Rahim, and B. Zhou, "Efficient denitrification and removal of natural organic matter, emerging pollutants simultaneously for RO concentrate based on photoelectrocatalytic radical reaction," *Separation and Purification Technology*, vol. 234, p. 116032, 2020.

[21] A. A. Nada, B. O. Orimolade, H. H. El-Maghrabi, B. A. Koiki, M. Rivallin, M. F. Bekheet, R. Viter, D. Damberga, G. Lesage, I. Iatsunskyi, *et al.*, "Photoelectrocatalysis of paracetamol on Pd–ZnO/N-doped carbon nanofibers electrode," *Applied Materials Today*, vol. 24, p. 101129, 2021.

[22] P. Alulema-Pullupaxi, L. Fernández, A. Debut, C. P. Santacruz, W. Villacis, C. Fierro, and P. J. Espinoza-Montero, "Photoelectrocatalytic degradation of glyphosate on titanium dioxide synthesized by sol-gel/spin-coating on boron doped diamond (TiO2/BDD) as a photoanode," *Chemosphere*, vol. 278, p. 130488, 2021.

[23] J. C. Cardoso, G. G. Bessegato, and M. V. B. Zanoni, "Efficiency comparison of ozonation, photolysis, photocatalysis and photoelectrocatalysis methods in real textile wastewater decolorization," *Water research*, vol. 98, pp. 39–46, 2016.

[24] R. B. Domínguez-Espíndola, J. C. Varia, A. Álvarez-Gallegos, M. L. Ortiz-Hernández, J. L. Peña-Camacho, and S. Silva-Martínez, "Photoelectrocatalytic inactivation of fecal coliform bacteria in urban wastewater using nanoparticulated films of TiO2 and TiO2/Ag," *Environmental technology*, vol. 38, no. 5, pp. 606–614, 2017.

[25] H. L. Tan, R. Amal, and Y. H. Ng, "Alternative strategies in improving the photocatalytic and photoelectrochemical activities of visible light-driven bivo 4: a review," *Journal of Materials Chemistry A*, vol. 5, no. 32, pp. 16498–16521, 2017.

[26] T. S. Dabodiya, P. Selvarasu, and A. V. Murugan, "Tetragonal to monoclinic crystalline phases change of bivo4 via microwave-hydrothermal reaction: in correlation with visible-light-driven photocatalytic performance," *Inorganic chemistry*, vol. 58, no. 8, pp. 5096–5110, 2019.

[27] S. Pu, Z. Yang, J. Tang, H. Ma, S. Xue, and Y. Bai, "Plasmonic silver/silver oxide nanoparticles anchored bismuth vanadate as a novel visible-light ternary photocatalyst for degrading pharmaceutical micropollutants," *Journal of Environmental Sciences*, vol. 96, pp. 21–32, 2020.

[28] M. J. Nalbandian, M. Zhang, J. Sanchez, Y.-H. Choa, D. M. Cwiertny, and N. V. Myung, "Synthesis and optimization of BiVO4 and co-catalyzed BiVO4 nanofibers for visible light-activated photocatalytic degradation of aquatic micropollutants," *Journal of Molecular Catalysis A: Chemical*, vol. 404, pp. 18–26, 2015.

[29] X. Gao, H. B. Wu, L. Zheng, Y. Zhong, Y. Hu, and X. W. Lou, "Formation of mesoporous heterostructured BiVO4/Bi2S3 hollow discoids with enhanced photoactivity," *Angewandte Chemie*, vol. 126, no. 23, pp. 6027–6031, 2014.

[30] F. F. Abdi, T. J. Savenije, M. M. May, B. Dam, and R. van de Krol, "The origin of slow carrier transport in BiVO4 thin film photoanodes: a time-resolved microwave conductivity study," *The Journal of Physical Chemistry Letters*, vol. 4, no. 16, pp. 2752–2757, 2013.

[31] S. Y. Chae, C. S. Lee, H. Jung, O.-S. Joo, B. K. Min, J. H. Kim, and Y. J. Hwang, "Insight into charge separation in WO3/BiVO4 heterojunction for solar water splitting," *ACS Applied Materials & Interfaces*, vol. 9, no. 23, pp. 19780–19790, 2017.

[32] Z. Guo, J. Wei, B. Zhang, M. Ruan, and Z. Liu, "Construction and photoelectrocatalytic performance of TiO2/BiVO4 heterojunction modified with cobalt phosphate," *Journal of Alloys and Compounds*, vol. 821, p. 153225, 2020.

[33] R. Saleh and N. F. Djaja, "Transition-metal-doped ZnO nanoparticles: synthesis, characterization and photocatalytic activity under UV light," *Spectrochimica Acta Part A: Molecular and Biomolecular Spectroscopy*, vol. 130, pp. 581–590, 2014.

[34] M. Norek, "Approaches to enhance UV light emission in ZnO nanomaterials," *Current Applied Physics*, vol. 19, no. 8, pp. 867–883, 2019.

[35] H. Khan, S. Samanta, M. Seth, and S. Jana, "Fabrication and photoelectrochemical activity of hierarchically porous tio2–zno heterojunction film," *Journal of Materials Science*, vol. 55, no. 26, pp. 11907–11918, 2020.

[36] P. Sahoo, A. Sharma, S. Padhan, and R. Thangavel, "Construction of zno@ nio heterostructure photoelectrodes for improved photoelectrochemical performance," *International Journal of Hydrogen Energy*, vol. 46, no. 73, pp. 36176–36188, 2021.

[37] C. Liu, F. Meng, L. Zhang, D. Zhang, S. Wei, K. Qi, J. Fan, H. Zhang, and X. Cui, "Cuo/zno heterojunction nanoarrays for enhanced photoelectrochemical water oxidation," *Applied Surface Science*, vol. 469, pp. 276–282, 2019.

[38] Z. Zeng, S. Chen, T. T. Y. Tan, and F.-X. Xiao, "Graphene quantum dots (GQDs) and its derivatives for multifarious photocatalysis and photoelectrocatalysis," *Catalysis Today*, vol. 315, pp. 171–183, 2018.

[39] J. Feng, H. Dong, L. Yu, and L. Dong, "The optical and electronic properties of graphene quantum dots with oxygen-containing groups: a density functional theory study," *Journal of Materials Chemistry C*, vol. 5, no. 24, pp. 5984–5993, 2017.

[40] Y. Yan, J. Gong, J. Chen, Z. Zeng, W. Huang, K. Pu, J. Liu, and P. Chen, "Recent advances on graphene quantum dots: from chemistry and physics to applications," *Advanced materials*, vol. 31, no. 21, p. 1808283, 2019.

[41] O. A. Arotiba, B. O. Orimolade, and B. A. Koiki, "Visible light–driven photoelectrocatalytic semiconductor heterojunction anodes for water treatment applications," *Current Opinion in Electrochemistry*, vol. 22, pp. 25–34, 2020.

[42] S. Meng, J. Zhang, S. Chen, S. Zhang, and W. Huang, "Perspective on construction of heterojunction photocatalysts and the complete utilization of photogenerated charge carriers," *Applied Surface Science*, vol. 476, pp. 982–992, 2019.

[43] J. Low, J. Yu, M. Jaroniec, S. Wageh, and A. A. Al-Ghamdi, "Heterojunction photocatalysts," *Advanced materials*, vol. 29, no. 20, p. 1601694, 2017.

[44] Y. Qin, S. Yang, X. You, Y. Liu, L. Qin, Y. Li, W. Zhang, and W. Liang, "Carbon nitride coupled with fe-based mofs as an efficient photoelectrocatalyst for boosted degradation of ciprofloxacin: Mechanism, pathway and fate," *Separation and Purification Technology*, p. 121325, 2022.

[45] Z. Wang, S. Xu, J. Cai, J. Ma, and G. Zhao, "Perspective on photoelectrocatalytic removal of refractory organic pollutants in water systems," *ACS ES&T Engineering*, 2022.

[46] C. Sima, C. Grigoriu, O. Toma, and S. Antohe, "Study of dye sensitized solar cells based on ZnO photoelectrodes deposited by laser ablation and doctor blade methods," *Thin Solid Films*, vol. 597, pp. 206–211, 2015.

[47] B. O. Orimolade, B. A. Koiki, G. M. Peleyeju, and O. A. Arotiba, "Visible light driven photoelectrocatalysis on a FTO/BiVO4/BiOI anode for water treatment involving emerging pharmaceutical pollutants," *Electrochimica Acta*, vol. 307, pp. 285–292, 2019.

[48] V. Sharma and P. K. Jha, "Enhancement in power conversion efficiency of edge-functionalized graphene quantum dot through adatoms for solar cell applications," *Solar Energy Materials and Solar Cells*, vol. 200, p. 109908, 2019.

[49] A. Raja, P. Rajasekaran, B. Vishnu, K. Selvakumar, J. Y. Do, M. Swaminathan, and M. Kang, "Fabrication of effective visible-light-driven ternary Z-scheme ZnO-Ag-BiVO4 heterostructured photocatalyst for hexavalent chromium reduction," *Separation and Purification Technology*, vol. 252, p. 117446, 2020.

[50] K. Zhang, Y. Liu, J. Deng, S. Xie, X. Zhao, J. Yang, Z. Han, and H. Dai, "Co–Pd/BiVO4: High-performance photocatalysts for the degradation of phenol under visible light irradiation," *Applied Catalysis B: Environmental*, vol. 224, pp. 350–359, 2018.

[51] Y. Wu, "Towards omps removal: Application of visible light driven heterojunction based BiVO4/BiOI photoanode for the degradation of paracetamol demineralized water," 2022.

[52] J. H. Kim, Y. H. Jo, J. H. Kim, and J. S. Lee, "Ultrafast fabrication of highly active BiVO4 photoanodes by hybrid microwave annealing for unbiased solar water splitting," *Nanoscale*, vol. 8, no. 40, pp. 17623–17631, 2016.

[53] A. Saranya, T. Devasena, H. Sivaram, and R. Jayavel, "Role of hexamine in ZnO morphologies at different growth temperature with potential application in dye sensitized solar cell," *Materials Science in Semiconductor Processing*, vol. 92, pp. 108–115, 2019.

[54] H. Slimani, N. Bessous, S. Dagher, A. Hilal-Alnaqbi, M. El Gamal, B. Akhozheya, and M. Mohammed, "Growth of ZnO nanorods on FTO glass substrate," *Materials Research Express*, vol. 7, no. 2, p. 025026, 2020.

[55] A. Pourrahimi, D. Liu, V. Ström, M. S. Hedenqvist, R. T. Olsson, and U. W. Gedde, "Heat treatment of ZnO nanoparticles: new methods to achieve high-purity nanoparticles for high-voltage applications," *Journal of Materials Chemistry A*, vol. 3, no. 33, pp. 17190–17200, 2015.

[56] D. A. Keller, H.-N. Barad, E. Rosh-Hodesh, A. Zaban, and D. Cahen, "Can fluorine-doped tin oxide, FTO, be more like indium-doped tin oxide, ITO reducing FTO surface roughness by introducing additional SnO2 coating," *Mrs Communications*, vol. 8, no. 3, pp. 1358–1362, 2018.

[57] J. Ji, P. Sang, and J. H. Kim, "Improving the photoelectrochemical performance of spin-coated WO3/BiVO4/ZnO photoanodes by maximizing charge transfer using an optimized ZnO decoration layer," *Ceramics International*, vol. 47, no. 18, pp. 26260–26270, 2021.

[58] X. Huang, J. Song, L. Wang, X. Gu, Y. Zhao, and Y. Qiang, "Photoelectrochemical properties of ZnO/BiVO4 nanorod arrays prepared through a facile spin-coating deposition route," *Materials Science in Semiconductor Processing*, vol. 97, pp. 106–111, 2019.

[59] C. Wu, R. Chen, C. Ma, R. Cheng, X. Gao, T. Wang, Y. Liu, P. Huo, and Y. Yan, "Construction of upconversion nitrogen doped graphene quantum dots modified BiVO4 photocatalyst with enhanced visible-light photocatalytic activity," *Ceramics International*, vol. 45, no. 2, pp. 2088–2096, 2019.

[60] J. S. Chang, Y. W. Phuan, M. N. Chong, and J. D. Ocon, "Exploration of a novel type ii 1D-ZnO nanorods/BiVO4 heterojunction photocatalyst for water depollution," *Journal of Industrial and Engineering Chemistry*, vol. 83, pp. 303–314, 2020.

[61] R. Pei, Z. Cheng, E. Wang, and X. Yang, "Amplification of antigen–antibody interactions based on biotin labeled protein–streptavidin network complex using impedance spectroscopy," *Biosensors and Bioelectronics*, vol. 16, no. 6, pp. 355–361, 2001.

[62] B. Appavu, S. Thiripuranthagan, S. Ranganathan, E. Erusappan, and K. Kannan, "BiVO4/N-rGO nano composites as highly efficient visible active photocatalyst for the degradation of dyes and antibiotics in eco system," *Ecotoxicology and environmental safety*, vol. 151, pp. 118–126, 2018.

[63] H. Li, Y. Sun, B. Cai, S. Gan, D. Han, L. Niu, and T. Wu, "Hierarchically Z-scheme photocatalyst of Ag@ AgCl decorated on BiVO4 (0 4 0) with enhancing photoelectrochemical and photocatalytic performance," *Applied Catalysis B: Environmental*, vol. 170, pp. 206–214, 2015.

[64] S. Kumar, A. Dhiman, P. Sudhagar, and V. Krishnan, "ZnO-graphene quantum dots heterojunctions for natural sunlight-driven photocatalytic environmental remediation," *Applied Surface Science*, vol. 447, pp. 802–815, 2018.

[65] S. Ni, T. Zhou, H. Zhang, Y. Cao, and P. Yang, "BiOI/BiVO4 two-dimensional heteronanostructures for visible-light photocatalytic degradation of rhodamine B," *ACS Applied Nano Materials*, vol. 1, no. 9, pp. 5128–5141, 2018.

[66] Y. Chen, Y. Liu, X. Xie, C. Li, Y. Si, M. Zhang, and Q. Yan, "Synthesis flower-like BiVO4/BiOI core/shell heterostructure photocatalyst for tetracycline degradation under visible-light irradiation," *Journal of Materials Science: Materials in Electronics*, vol. 30, no. 10, pp. 9311–9321, 2019.

[67] H. Dong, J. Li, M. Chen, H. Wang, X. Jiang, Y. Xiao, B. Tian, and X. Zhang, "High-throughput production of ZnO-MoS2-graphene heterostructures for highly efficient photocatalytic hydrogen evolution," *Materials*, vol. 12, no. 14, p. 2233, 2019.

[68] M. Wang, H. Yu, P. Wang, Z. Chi, Z. Zhang, B. Dong, H. Dong, K. Yu, and H. Yu, "Promoted photocatalytic degradation and detoxication performance for norfloxacin on Z-scheme phosphate-doped BiVO4/graphene quantum dots/P-doped g-c3n4," *Separation and Purification Technology*, vol. 274, p. 118692, 2021.

[69] C. Starr, C. Evers, and L. Starr, *Biology: concepts and applications*. Cengage Learning, 2014.

[70] T. K. Pathak, H. Swart, and R. Kroon, "Influence of Bi doping on the structure and photoluminescence of ZnO phosphor synthesized by the combustion method," *Spectrochimica Acta Part A: Molecular and Biomolecular Spectroscopy*, vol. 190, pp. 164–171, 2018.

[71] H. Li, X. He, Z. Kang, H. Huang, Y. Liu, J. Liu, S. Lian, C. H. A. Tsang, X. Yang, and S.-T. Lee, "Water-soluble fluorescent carbon quantum dots and photocatalyst design," *Angewandte Chemie International Edition*, vol. 49, no. 26, pp. 4430–4434, 2010.

[72] Y. Yan, Q. Liu, X. Du, J. Qian, H. Mao, and K. Wang, "Visible light photoelectrochemical sensor for ultrasensitive determination of dopamine based on synergistic effect of graphene quantum dots and TiO2 nanoparticles," *Analytica chimica acta*, vol. 853, pp. 258–264, 2015.

[73] N. Abdullayeva, C. T. Altaf, M. Mintas, A. Ozer, M. Sankir, H. Kurt, and N. D. Sankir, "Investigation of strain effects on photoelectrochemical performance of flexible ZnO electrodes," *Scientific reports*, vol. 9, no. 1, pp. 1–14, 2019.

[74] M. M. Mohamed, M. A. Ghanem, M. Khairy, E. Naguib, and N. H. Alotaibi, "Zinc oxide incorporated carbon nanotubes or graphene oxide nanohybrids for enhanced sonophotocatalytic degradation of methylene blue dye," *Applied Surface Science*, vol. 487, pp. 539–549, 2019.

[75] S. Kahng and J. H. Kim, "Heterojunction photoanode of SnO2 and mo-doped BiVO4 for boosting photoelectrochemical performance and tetracycline hydrochloride degradation," *Chemosphere*, vol. 291, p. 132800, 2022.

[76] M. Sousa, C. Gonçalves, V. J. Vilar, R. A. Boaventura, and M. Alpendurada, "Suspended TiO2-assisted photocatalytic degradation of emerging contaminants in a municipal wwtp effluent using a solar pilot plant with CPCs," *Chemical Engineering Journal*, vol. 198, pp. 301–309, 2012.

[77] J. Xu, H. Olvera-Vargas, B. J. H. Loh, and O. Lefebvre, "FTO-TiO2 photoelectrocatalytic degradation of triphenyltin chloride coupled to photoelectro-fenton: a mechanistic study," *Applied Catalysis B: Environmental*, vol. 271, p. 118923, 2020.

[78] L. Zhang, Y. Liu, and Y. Fu, "Degradation kinetics and mechanism of diclofenac by UV/peracetic acid," *RSC advances*, vol. 10, no. 17, pp. 9907–9916, 2020.

[79] F. Zietzschmann, C. Stützer, and M. Jekel, "Granular activated carbon adsorption of organic micro-pollutants in drinking water and treated wastewater–aligning breakthrough curves and capacities," *Water Research*, vol. 92, pp. 180–187, 2016.

[80] S. Liu, X. Zhao, H. Zeng, Y. Wang, M. Qiao, and W. Guan, "Enhancement of photoelectrocatalytic degradation of diclofenac with persulfate activated by cu cathode," *Chemical Engineering Journal*, vol. 320, pp. 168–177, 2017.

[81] B. Seger and P. V. Kamat, "Electrocatalytically active graphene-platinum nanocomposites. role of 2-D carbon support in PEM fuel cells," *The Journal of Physical Chemistry C*, vol. 113, no. 19, pp. 7990–7995, 2009.

[82] M. Li, Z. Chen, Z. Wang, and Q. Wen, "Investigation on degradation behavior of dissolved effluent organic matter, organic micro-pollutants and bio-toxicity reduction from secondary effluent treated by ozonation," *Chemosphere*, vol. 217, pp. 223–231, 2019.

[83] K. Gautam and S. Anbumani, "Ecotoxicological effects of organic micro-pollutants on the environment," in *Current developments in biotechnology and bioengineering*, pp. 481–501, Elsevier, 2020.

[84] P. Sun, T. Meng, Z. Wang, R. Zhang, H. Yao, Y. Yang, and L. Zhao, "Degradation of organic micropollutants in UV/NH2Cl advanced oxidation process," *Environmental Science & Technology*, vol. 53, no. 15, pp. 9024–9033, 2019.

[85] S. O. Ganiyu, S. Sable, and M. G. El-Din, "Advanced oxidation processes for the degradation of dissolved organics in produced water: A review of process performance, degradation kinetics and pathway," *Chemical Engineering Journal*, vol. 429, p. 132492, 2022.

[86] M. Montiel-Rozas, E. Madejón, and P. Madejón, "Effect of heavy metals and organic matter on root exudates (low molecular weight organic acids) of herbaceous species: An assessment in sand and soil conditions under different levels of contamination," *Environmental Pollution*, vol. 216, pp. 273–281, 2016.

[87] F. Zhao, W. Li, Y. Song, Y. Fu, X. Liu, C. Ma, G. Wang, X. Dong, and H. Ma, "Constructing S-scheme Co3O4-C3N4 catalyst with superior photoelectrocatalytic efficiency for water purification," *Applied Materials Today*, vol. 26, p. 101390, 2022.

[88] Z. Liu, Y. Song, Q. Wang, Y. Jia, X. Tan, X. Du, and S. Gao, "Solvothermal fabrication and construction of highly photoelectrocatalytic TiO2 NTs/Bi2MoO6 heterojunction based on titanium mesh," *Journal of colloid and interface science*, vol. 556, pp. 92–101, 2019.

Appendix A

Trapping experiments

Table A.1: Concentrations of other common pollutants before and after degradation experiments in spiked MiliQ.

OMPs Name	p-benzoquinone in spiked effluent TD (%)	$ZnO/BiVO_4$ in spiked effluent TD (%)	Methanol in spiked effluent TD (%)
1. BTA	-	52.31	44.42
2. MBTA	-	53.45	44.84
3. CBZ	8.95	46.22	31.66
4. DIC	24.96	99.76	99.57
5. HCTZ	-	100.00	99.28
6. MP	11.21	41.99	29.22
7. SMX	-	61.54	27.54
8. PRO	-	91.02	84.79
9. SOT	-	91.39	80.93
10. TMP	-	55.88	31.00
11. CLA	42.32	49.48	-

'-' means the OMP reacted with the scavengers, and incorrect data was observed.

Two trapping experiments were carried out in this study. Firstly, 5 mM p-benzoquinone was added to the solution as a scavenger to remove $\cdot O_2^-$ produced by photoanode in the PEC process. Secondly, 5 mM methanol was added to the solution as a scavenger to remove $\cdot OH$. The results of the total degradations are shown in Table A.1. Because the p-benzoquinone and methanol reacted with some OMPs, only the results of CBZ, DIC and MP were reliable. For these three OMPs, the total degradation efficiencies were lower for p-benzoquinone compared to methanol. Therefore, the findings indicated two results. First of all, both $\cdot O_2^-$ and $\cdot OH$ were produced by the PEC process. In the meantime, $\cdot O_2^-$ was the active species that dominated OMP degradation.

Appendix B

SEM images

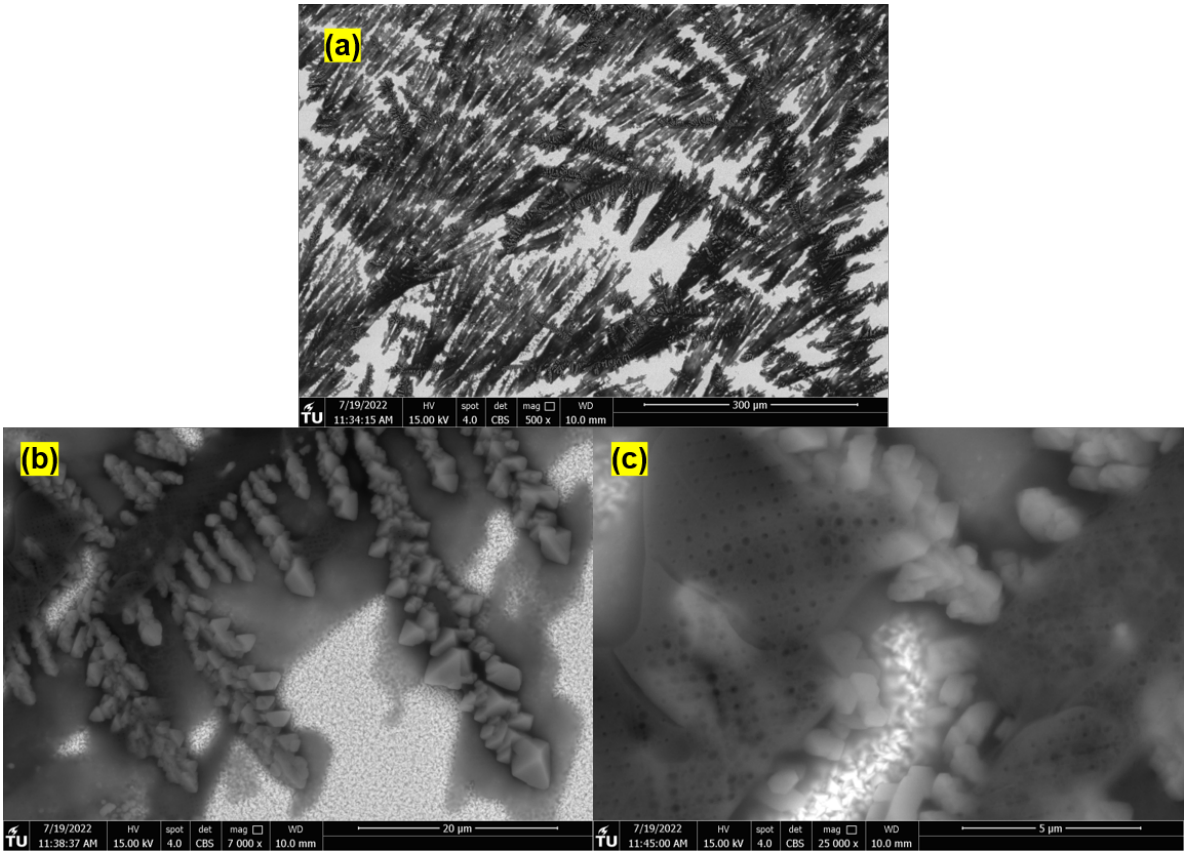

FIGURE B.1: Low and high magnification SEM images of (a) 500x, (b) 7 000x, (c) 25 000x GDs on FTO glass.

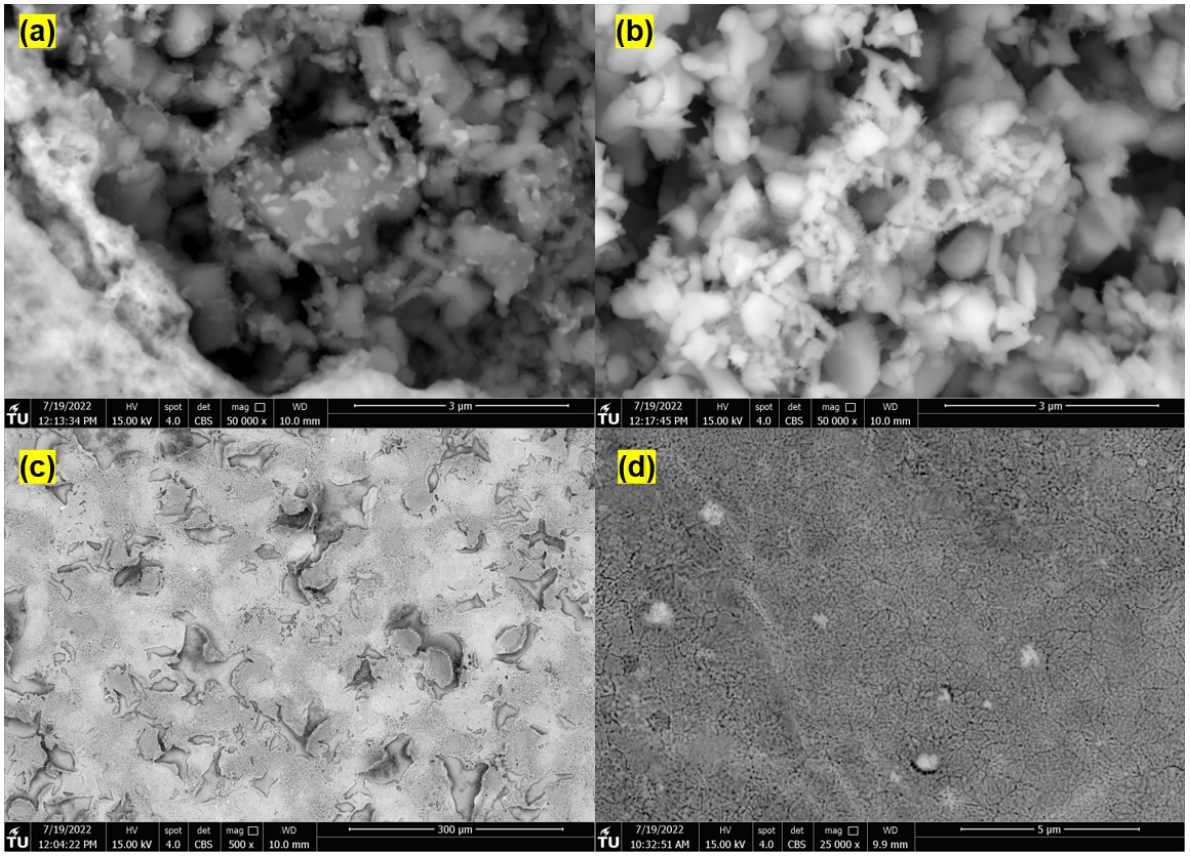

FIGURE B.2: Low and high magnification SEM images of (a) and (b) 50 000x, (c) 500x $ZnO/BiV0_4$ film, (d) 25 000x compact $BiV0_4$ film.